

SYNTHESIS AND STRUCTURE AFFINITY RELATIONSHIP OF SMALL MOLECULES FOR IMAGING HUMAN CD80 BY POSITRON EMISSION TOMOGRAPHY

Marco Francesco Taddio, Linjing Mu, Claudia Adrianna Castro Jaramillo,
Tanja Bollmann, Dominik Schmid, Lukas Muskalla, Tim Gruene, Aristeidis
Chiotellis, Simon Mensah Ametamey, Roger Schibli, and Stefanie D. Krämer

J. Med. Chem., **Just Accepted Manuscript** • DOI: 10.1021/acs.jmedchem.9b00858 • Publication Date (Web): 20 Aug 2019

Downloaded from pubs.acs.org on August 21, 2019

Just Accepted

“Just Accepted” manuscripts have been peer-reviewed and accepted for publication. They are posted online prior to technical editing, formatting for publication and author proofing. The American Chemical Society provides “Just Accepted” as a service to the research community to expedite the dissemination of scientific material as soon as possible after acceptance. “Just Accepted” manuscripts appear in full in PDF format accompanied by an HTML abstract. “Just Accepted” manuscripts have been fully peer reviewed, but should not be considered the official version of record. They are citable by the Digital Object Identifier (DOI®). “Just Accepted” is an optional service offered to authors. Therefore, the “Just Accepted” Web site may not include all articles that will be published in the journal. After a manuscript is technically edited and formatted, it will be removed from the “Just Accepted” Web site and published as an ASAP article. Note that technical editing may introduce minor changes to the manuscript text and/or graphics which could affect content, and all legal disclaimers and ethical guidelines that apply to the journal pertain. ACS cannot be held responsible for errors or consequences arising from the use of information contained in these “Just Accepted” manuscripts.

SYNTHESIS AND STRUCTURE AFFINITY RELATIONSHIP OF SMALL MOLECULES FOR IMAGING HUMAN CD80 BY POSITRON EMISSION TOMOGRAPHY

Marco F. Taddio^{1*}, Linjing Mu^{1,2}, Claudia A. Castro Jaramillo¹, Tanja Bollmann¹, Dominik Schmid¹, Lukas Muskalla³, Tim Grüne^{3,4}, Aristeidis Chiotellis¹, Simon M. Ametamey¹, Roger Schibli¹, Stefanie D. Krämer^{1*}

¹ Center for Radiopharmaceutical Sciences ETH, PSI and USZ, Department of Chemistry and Applied Biosciences, ETH Zurich, CH-8093 Zurich, Switzerland; ² Department of Nuclear Medicine, University Hospital Zurich, CH-8091 Zurich, Switzerland; ³ Laboratory for Catalysis and Sustainable Chemistry, Paul Scherrer Institute, CH-5232 Villigen PSI, Switzerland; ⁴ X-ray Structure Analysis Centre, Faculty of Chemistry, University of Vienna, A-1090 Vienna, Austria

Keywords: CD80 / imaging / inflammation / PET / small molecules

Abstract

The co-stimulatory molecule CD80 is an early marker for immune activation. It is upregulated on activated antigen-presenting cells. We aimed at developing a tracer for imaging CD80 by positron emission tomography (PET). Novel CD80 ligands were synthesized and tested by SPR for affinity to human CD80 (hCD80) and displacement of endogenous ligands. Several compounds bound with one-digit nanomolar affinity to hCD80 and displaced CTLA-4 and CD28 at nanomolar concentrations. A structure-affinity relationship study revealed relevant moieties for strong affinity to hCD80 and positions for further modifications. Lead compound MT107 (**7f**) was radiolabelled with carbon-11. *In vitro*, [¹¹C]MT107 showed specific binding to hCD80-positive tissue and high plasma protein binding. *In vivo*, [¹¹C]MT107 accumulated in liver, gall bladder and intestines, but only scarcely in hCD80-positive xenografts. The unfavourable *in vivo* performance may result from high plasma protein binding and extensive biliary excretion.

1
2
3 ABSTRACT
4
5
6

7 The co-stimulatory molecule CD80 is an early marker for immune activation. It is upregulated on
8 activated antigen-presenting cells. We aimed at developing a tracer for imaging CD80 by positron
9 emission tomography (PET). Novel CD80 ligands were synthesized and tested by SPR for affinity
10 to human CD80 (hCD80) and displacement of endogenous ligands. Several compounds bound
11 with one-digit nanomolar affinity to hCD80 and displaced CTLA-4 and CD28 at nanomolar
12 concentrations. A structure-affinity relationship study revealed relevant moieties for strong affinity
13 to hCD80 and positions for further modifications. Lead compound MT107 (**7f**) was radiolabelled
14 with carbon-11. *In vitro*, [¹¹C]MT107 showed specific binding to hCD80-positive tissue and high
15 plasma protein binding. *In vivo*, [¹¹C]MT107 accumulated in liver, gall bladder and intestines, but
16 only scarcely in hCD80-positive xenografts. The unfavourable *in vivo* performance may result
17 from high plasma protein binding and extensive biliary excretion.
18
19
20
21
22
23
24
25
26
27
28
29
30
31
32
33
34
35
36
37
38
39
40
41
42
43
44
45
46
47
48
49
50
51
52
53
54
55
56
57
58
59
60

INTRODUCTION

The co-stimulatory molecules CD80 (B7-1) and CD86 (B7-2) are expressed on activated antigen-presenting cells. They interact with immune-modulatory molecules on T cells, among them CTLA-4 and CD28. The weak-affinity interaction of CD80 or CD86 with CD28 is involved in T-cell activation, while the strong interaction of CD80/CD86 with CTLA-4 prevents T-cell activation.^{1,2,3}

The balance between T cell activation and inactivation is disturbed in various diseases including cancer⁴, atherosclerosis^{5,6}, autoimmune diseases⁷ and transplant rejection⁸. Several therapeutic strategies aim at modulating the levels or functions of the co-stimulatory molecules accordingly.

CD80/CD86 and their receptors are targeted by immunotherapies for various indications.^{9,10}

However, following their dual functionality, finding the right balance in CD80/CD86 modulation remains challenging. Diagnosis, disease staging and therapy planning may benefit from a non-invasive method to detect and quantify T-cell activating co-stimulatory molecules in tissue.

Several fusion proteins are on the market which bind to CD80 and CD86 with strong affinity leading to co-stimulation blockade and anergy of T cells. Abatacept and belatacept are successfully used in rheumatoid arthritis^{9,10} and for the prophylaxis of organ rejection in transplantation medicine, respectively.^{11,12} Both are fusion proteins of the extracellular domain of CTLA-4 and the IgG Fc part. Belatacept contains two pointmutations in the binding domains which result in a 2-fold stronger affinity to human CD80 and a 4-fold stronger affinity to human CD86 as compared to abatacept.¹¹

Low molecular weight compounds with strong affinities to CD80 were developed to overcome the drawback of negligible oral bioavailability of the fusion proteins.^{13,14,15,16} Erbe *et al.* discovered a binding site for small molecules on human CD80 (hCD80) which is adjacent to the binding domains for CTLA-4 and CD28, respectively.¹³ The small-molecule binding site is absent on

1
2
3 rodent CD80 as concluded from both the amino acid sequence and absence of strong-affinity
4 binding of the low molecular weight ligands of hCD80.¹³ In the year 2004, Huxley *et al.* published
5 structures with strong affinities and high selectivity for hCD80 over hCD86.¹⁵
6
7

8
9
10 Previous work from our group with a carbon-11 labelled radiotracer (¹¹C]AM7), based on the lead
11 structure from Huxley *et al.*¹⁵ (**1** in Fig. 1), showed promising results in *in vitro* autoradiography
12 experiments with hCD80-positive xenograft and human atherosclerotic plaque tissue slices.
13 However, it had unfavourable pharmacokinetic properties in mice with high plasma protein
14 binding (human and mouse) and substantial biliary excretion. *In vivo* accumulation in a hCD80-
15 positive xenograft was poor.⁶
16
17
18
19
20
21
22
23

24
25 In this study, we explored the potential of structurally modified CD80 ligands for the development
26 of a PET tracer with altered pharmacokinetics. We increased the structural diversity by
27 hybridisation of the lead structures introduced by Huxley *et al.*¹⁵ and Green *et al.*¹⁴ and
28 investigated the structure-affinity relationship of the new compounds by surface plasmon
29 resonance (SPR). A ligand combining core-structure modifications and strong affinity was labelled
30 with carbon-11 and evaluated by PET/CT in mice with hCD80-positive Raji xenografts.
31
32
33
34
35
36
37
38
39
40
41
42
43
44
45
46
47
48
49
50
51
52
53
54
55
56
57
58
59
60

RESULTS

Chemistry. A cinnoline-based compound (**1**)¹⁵ and pyrazolopyridine-based compounds (**2**, **3**)¹⁴ were previously reported as potent small molecule ligands for hCD80. Based on these core structures, we designed and synthesized novel cinnoline-, quinoline- and pyrazolopyridine-based compounds in this work. Replacement of the methyl-pyrazole moiety of compound **2** with the benzene ring of compound **1** led to novel quinoline-based compounds **7e-g** (Figure 1). The acid intermediates were included for comparison with the acid compound **3**.

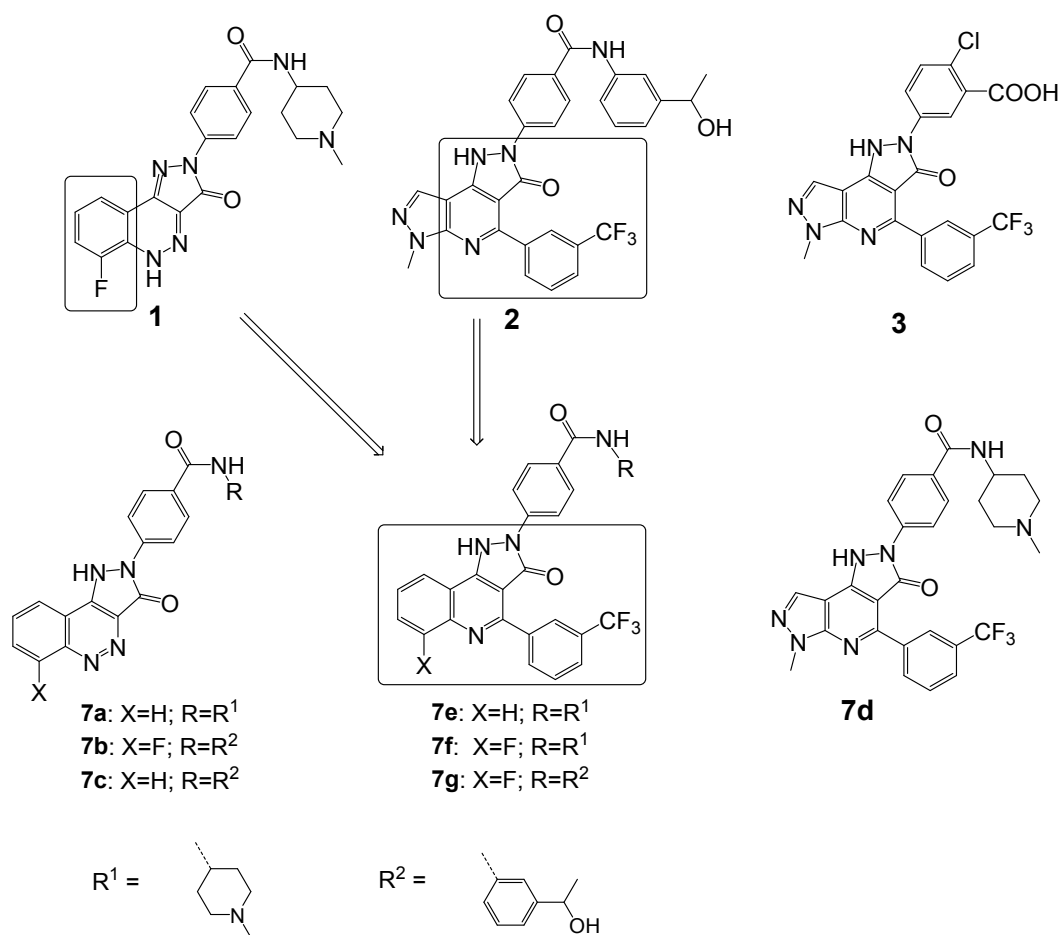
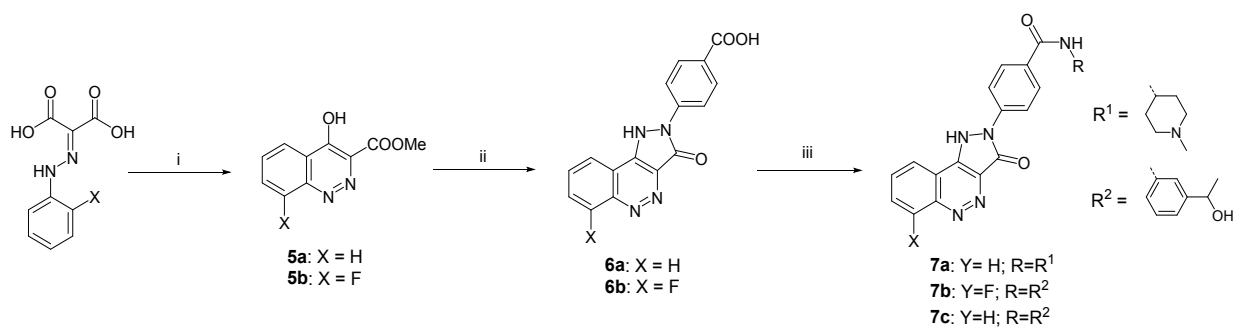


Figure 1. Structures of the synthesized compounds. Boxes indicate structural features from reported compounds (**1** & **2**) which were conserved in hybrid compounds **7e** – **7g**.

Three series of cinnoline-, quinoline- and pyrazolopyridine-based compounds were synthesized based on the modified synthetic procedures as previously described.^{14,15} Scheme 1 depicts the synthetic route for cinnoline-based compounds. Compounds **5a** and **5b** were synthesized by reacting their corresponding phenylhydrazonomalonic acid with thionylchloride, cyclization and methyl ester formation in the presence of TiCl₄ and methanol. Converting the hydroxyl group to the chlorinated intermediate, then reacting with 4-hydrazino-benzoic acid formed the key acid compounds **6a** and **6b** in more than 75% yields. Subsequently, coupling with 1-methylpiperidin-4-amine or 1-(3-aminophenyl)ethan-1-ol afforded compounds **1** and **7a-c** in moderate yields.

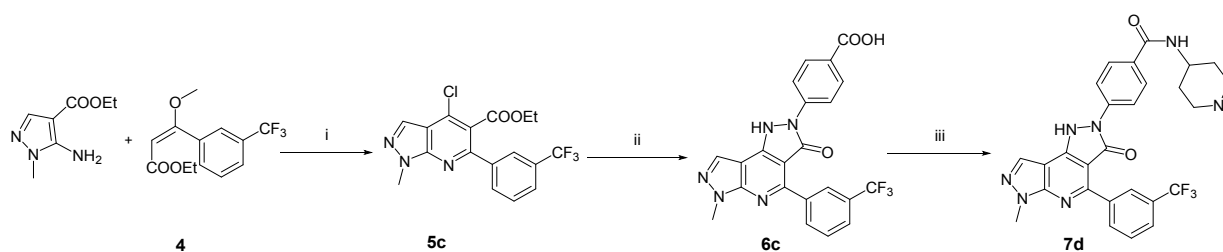
Scheme 1: Synthetic pathway towards cinnoline-based compounds.



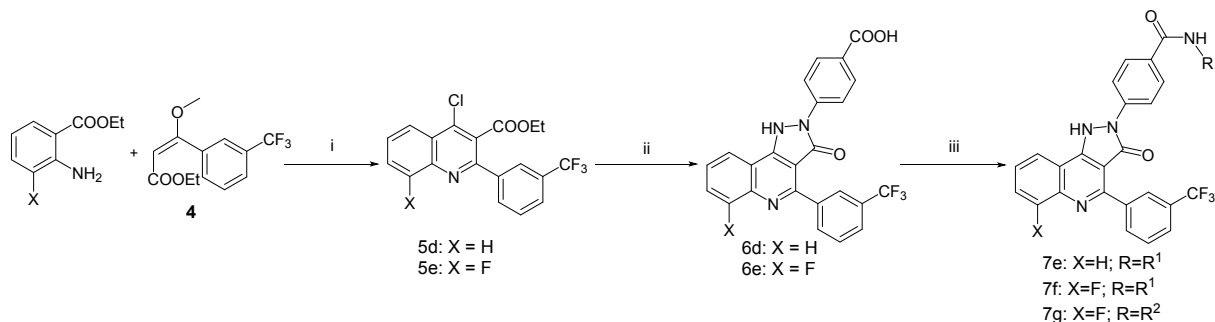
Reagents and conditions: (i) 1) SOCl₂, 80°C; 2) TiCl₄, 110°C; 3) MeOH, 60°C; (ii) 1) SOCl₂, 80°C, 1 h; 2) 4-hydrazinylbenzoic acid, 70°C, EtOH, 1 h; (iii) R-NH₂, EDC, DIPEA, rt, DMF, 18 h. R¹, R², see Figure 1.

The pyrazolopyridine- and quinoline-based compounds were synthesized as illustrated in Scheme 2 and 3, respectively. Compound **4** was synthesized by heating ethyl 3-(trifluoromethyl)benzoate in EtOAc with sodium hydride and subsequent methylation with trimethylsilyldiazomethane at room temperature with 48% yield. Gould-Jacobs cyclisation with ethyl 3-methoxy-3-(3-(trifluoromethyl)phenyl)acrylate (**4**) under strong basic conditions, followed by substitution of the hydroxy group by chlorine using phosphorous oxychloride, afforded 1-methyl-1*H*-pyrazolo[3,4-*b*]pyridine (**5c**) or quinolines (**5d**, **5e**) with 55-61% yields. Subsequent Knorr pyrazole ring formation with hydrazinyl benzoic acid derivatives under basic conditions and heating afforded compounds **6c-e** in 66-85% and compound **3** in 31% yield. In the last step, the carboxylic acid was activated with a coupling reagent (EDC hydrochloride or HATU) and two different building blocks (*meta*-1-hydroxyethyl-phenyl or *para*-1-methylpiperidinyl) were introduced by amide bond formation in 13-87% yields (**2**, **7d-g**).

Scheme 2: Synthetic route for pyrazolopyridine-based compound **7d**.



Reagents and conditions: (i) 1) NaH, reflux, THF, 16 h; 2) POCl₃, 120°C, 2 h; (ii) 4-hydrazinylbenzoic acid, NaOtBu, 100°C, ethylene glycol, 18 h; (iii) 1-methylpiperidin-4-amine, EDC, DIPEA, rt, DMF, 18 h

Scheme 3: Synthetic pathway toward quinoline-based compounds.

Reagents and conditions: (i) 1) NaH, reflux, THF, 16 h; 2) POCl₃, 120°C, 2 h; (ii) 4-hydrazinylbenzoic acid, NaO^tBu, 100°C, ethylene glycol, 18 h; (iii) R-NH₂, HATU, DIPEA, rt, DMF, 30 min. R¹, R², see Figure 1.

Table 1: Synthesized compounds (structures and substituents according to Figure 1 and Scheme 1) and their affinity to hCD80 determined by surface plasmon resonance.

Compound	X	R	$K_d \pm SD$ [nM] (<i>n</i>)
1 (AM7)	F	R ¹	3.8 ± 2.5 (9)
2	-	R ²	142 ± 61 (3)
3	-	-	90.7, 48.4 (2)
6a	H	-	572, 368 (2)
6b	F	-	n.d.
6c	-	-	308, 397 (2)
6d	H	-	194 (1)
6e	F	-	n.d.
7a	H	R ¹	9.3, 10.7 (2)
7b	F	R ²	120, 72 (2)
7c	H	R ²	117, 310 (2)
7d	-	R ¹	109 ± 10 (3)
7e	H	R ¹	7.1, 6.5 (2)
7f (MT107)	F	R ¹	4.2 ± 2.3 (9)
7g	F	R ²	113 ± 50 (4)

1
2
3 (*n*), number of experiments; SD, standard deviation; n.d., not determined. K_d values of individual
4 experiments are shown for $n \leq 2$. R^1 , R^2 , see Figure 1.
5
6
7
8
9

10 **Binding to hCD80.** After the synthesis of the unlabelled compounds in Table 1, we investigated
11 their affinity and kinetics for the binding to recombinant hCD80 (rhCD80) by SPR. Typical
12 binding curves are shown in Supplementary Figure S1. The calculated binding rate constant (k_{on})
13 ranged from 9×10^4 to 7×10^5 $M^{-1}s^{-1}$. The dissociation rate constant (k_{off}) ranged from 4×10^{-4} to 0.4
14 s^{-1} and K_d from 3.8 to 572 nM (Table 1). In order to reach high signal ratios between hCD80-
15 positive and negative tissues in PET imaging, we aimed at a strong affinity (low K_d) with a low
16 k_{off} . This is the case for compounds in the right upper corner in the plot $1/K_d$ vs $1/k_{off}$ in Figure 2
17
18
19
20
21
22
23
24
25
26
27 **(1, 7a, 7e, 7f).**
28
29
30
31
32
33
34
35
36
37
38
39
40
41
42
43
44
45
46
47
48
49
50
51
52
53
54
55
56
57
58
59
60

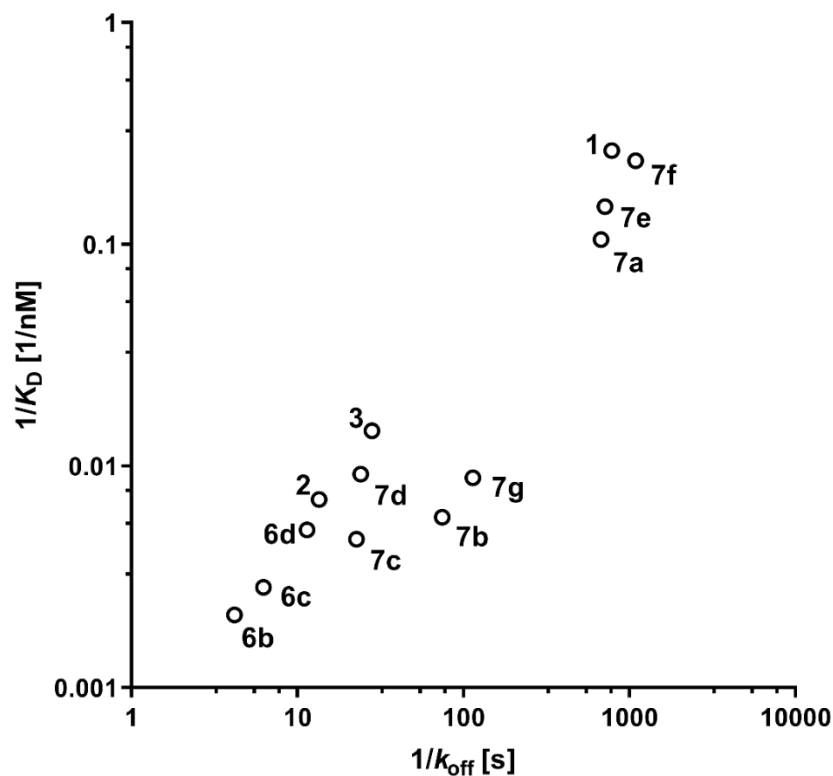


Figure 2. $1/K_d$ plotted against $1/k_{off}$ from SPR experiments. Compounds with preferred binding properties for PET imaging are in the upper right corner (low K_d , low k_{off}).

Displacement of hCTLA-4 and hCD28 from hCD80 binding. We next investigated by SPR the potential of **1**, **2** and **7f** for displacing the binding domains of hCTLA-4 (in our study abatacept) and rhCD28 from the binding to rhCD80. We first confirmed published K_d values of rhCTLA-4 (0.27 nM) and rhCD28 (16.3 nM) to rhCD80.¹⁷ In our assay, they were 0.5 nM and 17.8 nM, respectively ($n = 1$). For the displacement assay, we used abatacept and rhCD28 at concentrations 3-4-fold above their K_d values, *i.e.*, 2 nM and 50 nM, respectively. According to the Cheng-Prusoff equation, keeping a constant ratio between concentration and K_D of a displaced ligand (abatacept) should result in similar IC_{50} values for a particular displacer compound in varying experiments.

1
2
3 The displacement of abatacept was most effective by **1** and **7f** with IC_{50} values around
4 15 nM (Figure 3). The IC_{50} was more than one magnitude higher for **2**. The IC_{50} values for the
5 displacement of rhCD28 were around 10 nM for **1** and **7f**, as shown in Figure 3 (not determined
6 for **2**). The respective K_i values calculated from these data are shown in Figure 3. The K_i
7 determined in the displacement experiments were in agreement with the K_d values determined in
8 the direct binding experiments (Table 1). Furthermore, **7f** competed only weakly (at
9 concentrations $> 50 \mu\text{M}$) with the binding of abatacept to rhCD86 and recombinant murine CD80
10 (rmCD80), in agreement with its selectivity for hCD80 over hCD86 and mCD80 (Supplementary
11 Figures S2 and S3).
12
13
14
15
16
17
18
19
20
21
22
23
24
25
26
27
28
29
30
31
32
33
34
35
36
37
38
39
40
41
42
43
44
45
46
47
48
49
50
51
52
53
54
55
56
57
58
59
60

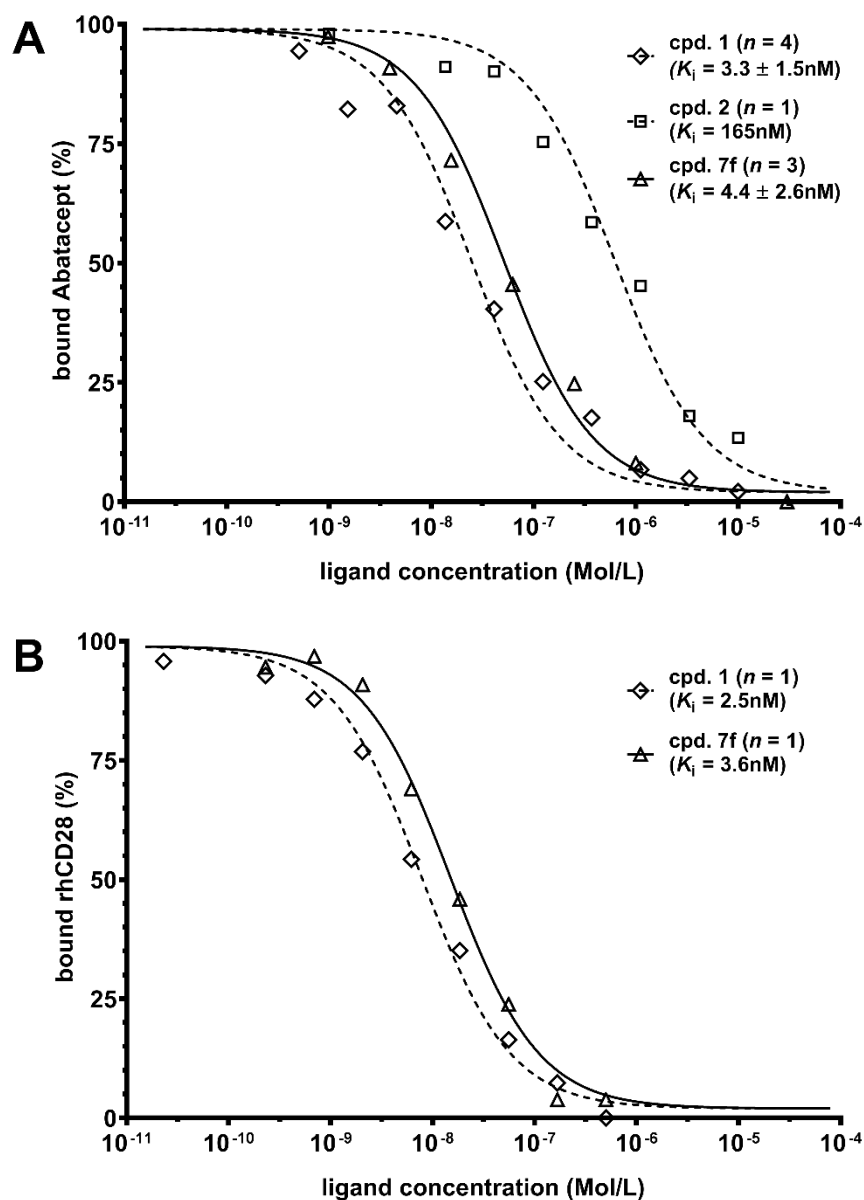


Figure 3: Representative displacement curves of (A) 2 nM abatacept or (B) 50 nM rhCD28 from immobilized rhCD80 by small molecules **1**, **2** (only in A) or **7f**. IC₅₀ values were determined from the displacement by different concentrations of synthesized small molecules (x axis) assuming 1:1 binding stoichiometries. The respective (averaged) K_i values (± S.D. for n ≥ 3) are indicated in the Figure. n, number of experiments for K_i determination.

1
2
3
4
5
6 **Radiosynthesis of [¹¹C]1 and [¹¹C]7f.** Precursor compounds for radiolabelling were synthesized
7
8 from intermediates **6b** and **6e** (shown in Scheme 1 and 3, respectively). By activation of the
9
10 carboxylic acid with the coupling reagent EDC and following amide bond formation 1-boc-
11
12 piperidin-4-amine under basic conditions, a boc-protected piperidine was introduced which was
13
14 subsequently deprotected with DCM/TFA to afford compounds **8a** and **8b** in good yields (details
15
16 in experimental section). Our group recently described the radiolabelling procedure of **1** with
17
18 carbon-11 (ref. 6). This procedure was applied for the radiosynthesis of both [¹¹C]**1** and our new
19
20 radiotracer [¹¹C]**7f**. Details on the one-step radiosynthesis are described in the experimental
21
22 section. Molar activities at the end of synthesis were between 200 and 500 GBq/μmol for [¹¹C]**1**
23
24 and between 20 and 80 GBq/μmol for [¹¹C]**7f**.
25
26
27
28
29
30
31

32 **Lipophilicity, membrane permeability & plasma protein binding.** *In vivo*, [¹¹C]**1** scarcely
33
34 distributed to the tissue, in agreement with its low log *D* at pH 7.4 of 0.1 and its low free fraction
35
36 in plasma of 0.02.⁶ We determined log *D* of [¹¹C]**7f** at various pH. **7f** differs from **1** by the C-[3-
37
38 (trifluoromethyl)phenyl] moiety replacing the nitrogen in position 2 of the cinnoline substructure
39
40 (Figure 1 and Table 1). As expected, this modification rendered the compound more lipophilic,
41
42 with a log *D* at pH 7.4 of 1.98 ± 0.06. The log *D* was significantly lower at pH 5.4 than at higher
43
44 pH values (Supplementary Figure S4). This is in agreement with the distribution characteristics of
45
46 a basic compound (tertiary amine in R², Figure 1). The fit log *P* was 2.1 with a fit p*K*_a of 7.1.
47
48

49
50
51 We furthermore investigated the potential of the synthesized compounds **1**, **2**, **7e**, **7f** and **7g** to cross
52
53 lipid bilayers at pH 7.4, using a recently introduced liposomal fluorescent permeability assay.¹⁸
54
55
56
57
58
59
60

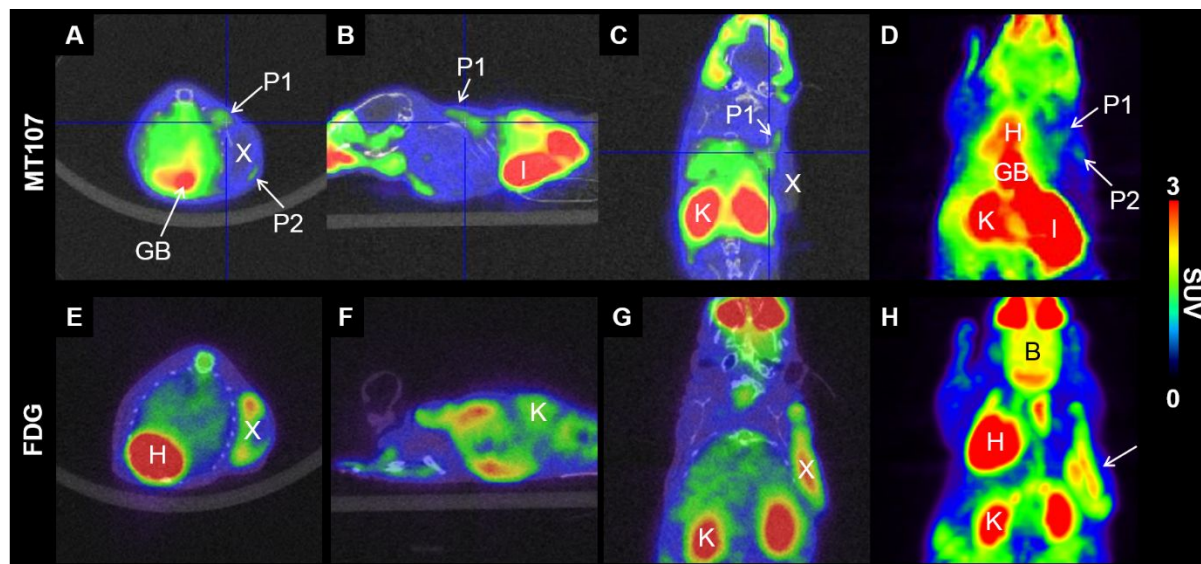
1
2
3 The logarithmic permeability coefficients, $\log(P_{\text{FLipP}}$, cm/s), ranged from -6.7 to -5.4, indicating
4 poor to moderate membrane permeability.¹⁸ Permeation kinetics were fastest for **1**, **7e** and **7f** with
5
6 $\log P_{\text{FLipP}}$ above -6.
7
8
9

10 The plasma protein binding of [¹¹C]**7f** was investigated with human plasma and bovine serum
11 albumin (BSA) using ultracentrifugation filter units. The free fraction was 0.023 ± 0.002 ($n = 4$)
12 for human plasma which is similar to the plasma protein binding of [¹¹C]**16**, and a higher free
13 fraction for BSA of 0.159 ± 0.002 ($n = 3$).
14
15
16
17
18
19
20
21
22

23 **In vitro autoradiography.** We chose compound **7f** for further *in vitro* and *in vivo* evaluation based
24 on its strong binding affinity to hCD80 (low K_d) at low k_{off} (Figure 2 and Supplementary Figure
25 S1) and as it differed from **1** in at least one physicochemical property (higher lipophilicity).
26 Structural modifications with higher predicted impact on the physicochemical properties (*e.g.*,
27 protonation/deprotonation equilibria) resulted in weakened binding affinity (Figures 1, 2 and
28 Table 1). *In vitro* autoradiography with [¹¹C]**7f** revealed higher accumulation on tissue slices of
29 hCD80-positive Raji than hCD80-negative NCI-H69 xenografts (Supplementary Figures S5 and
30 S6). The binding of [¹¹C]**7f** to hCD80-positive Raji xenograft slices was reduced by an excess of
31 5 μM **7f**, **1**, **2** and abatacept, respectively, by around 35% of the total binding. No reduction in
32 [¹¹C]**7f** binding was observed with the hCD80-negative tissue slices under these blocking
33 conditions.
34
35
36
37
38
39
40
41
42
43
44
45
46
47
48
49
50

51 **In vivo evaluation in Raji xenograft bearing mice.** We further evaluated [¹¹C]**7f** *in vivo* by
52 PET/CT imaging. We have recently compared the *in vivo* pharmacokinetics of [¹¹C]**1** and [¹¹C]**7f**
53
54
55
56
57
58
59
60

1
2
3 by kinetic modelling with PET data.¹⁹ Both tracers showed low distribution to tissue, in agreement
4 with the high plasma protein binding, but high extraction into the bile relative to the low free
5 fraction in plasma. This resulted in high abdominal radioactivity with spill-over to peripheral
6 tissues in the PET images. The biliary excretion of [¹¹C]7f was significantly reduced by pre-
7 administration of cyclosporine, an inhibitor of several hepatic transport proteins.¹⁹ Here, we
8 evaluated the uptake of [¹¹C]7f into the Raji xenografts from the data sets which were used for
9 pharmacokinetic modelling in the previous work.¹⁹ Figure 4 shows [¹¹C]7f PET images of a Raji
10 xenograft bearing SCID mouse after administration of cyclosporine ~30 min before the tracer.
11 Scarce accumulation of [¹¹C]7f in the periphery of the xenograft, as indicated in Figure 4, was
12 observed in two out of four cyclosporine-administered animals. No xenograft accumulation was
13 observed in the four animals without cyclosporine. For comparison, Figure 4 shows in addition a
14 representative [¹⁸F]FDG scan of a Raji-xenograft bearing mouse.



34
35
36
37
38
39
40
41
42
43
44
45
46
47
48
49
50
51
52 **Figure 4:** PET/CT images of a Raji (hCD80+) xenograft bearing mouse after tail vein injection of
53 11.7 MBq (13 nmol/kg) [¹¹C]7f, 30 min after i.v. injection of 50 mg/kg cyclosporine (A-D). (E-H)

1
2
3 For comparison, representative PET/CT images of a Raji (hCD80+) xenograft bearing mouse after
4 tail vein injection of 8.6 MBq [¹⁸F]FDG. Transversal (A,E), sagittal (B,F) and coronal (C,G)
5
6 planes, as indicated by the blue cross hairs. (D,H) Maximal intensity projection. CT, grey scale;
7
8 PET, color scale. H, blood pool (heart); GB, gall bladder; I, intestines; K, kidney; B, brain; P1 and
9
10 P2, peripheral locations of the xenograft with potential tracer accumulation; X, Raji xenograft.
11
12 SUV, standardised uptake value. Note that this scan was used for pharmacokinetic modelling in
13
14 our previous work¹⁹ and that different animals were used for the [¹¹C]7f and the [¹⁸F]FDG scan.
15
16
17
18
19
20
21
22

23 In order to evaluate the viability of the tumor cells and their general accessibility by radiotracers,
24 additional mice with Raji xenografts were scanned with the glucose analogue [¹⁸F]FDG. [¹⁸F]FDG
25
26 uptake was substantial in major parts of the xenografts (Figure 4), confirming the presence of
27
28 viable tumor tissue. The *in vivo* expression of hCD80 and its localisation on the cell surface were
29
30 confirmed by flow cytometry and RT-qPCR (Supplementary Figures S7 and S8).
31
32
33
34

35 The metabolic stability of [¹¹C]7f was investigated in xenograft-free C57BL/6 mice. Only parent
36
37 tracer was detected in blood plasma, bile and urine 15 min after tracer i.v. injection (Supplementary
38
39 Figure S9).
40
41
42
43
44

45 DISCUSSION

46
47
48 Our SPR data from a set of novel structures revealed that the methylpiperidine moiety is an
49
50 essential part for the strong binding to hCD80. Compounds with the N-methyl-piperidine moiety
51
52 (**1**, **7a**, **7e**, **7f**) showed consistently stronger affinities than compounds with the phenylethan-1-ol
53
54 moiety. In addition, the cinnoline- and quinoline-based structures showed stronger binding than
55
56
57
58
59
60

1
2
3 the pyrazolopyridine-based structures. The modification with an additional CF₃-substituted phenyl
4 ring in position 2 of the quinoline ring system did not affect the binding affinity to hCD80. This
5 suggests that this part of the structure is tolerant for modifications, as was seen for novel structure
6 **7f**, which showed similar affinity as **1** despite an additional bulky group (CF₃ substituted aromatic
7 ring). Taken together, the structure affinity relationship study with hybrid structures of **1** and **2**
8 provides new insights in the structural requirements for CD80 binding and indicates that further
9 modifications are possible without affinity loss.

10
11 Displacement of rhCTLA-4 and rhCD28 from hCD80 by **1** and **7f** showed that this low molecular
12 weight compound class has the potential to displace large proteins from binding to hCD80. This
13 ability may be attained by an allosteric mechanism, due to adjacent binding sites on the tertiary
14 structure of hCD80.¹³

15
16 The experimental log *D* at pH 7.4 of [¹¹C]**7f** was two log units higher than that of [¹¹C]**1**. However,
17 lipid bilayer permeation of both compounds **1** and **7f** was poor to moderate. In addition, both had
18 similar high plasma protein binding with a free fraction in plasma of ~ 0.02 (Müller et al.⁶ and this
19 study). The free fraction of [¹¹C]**7f** in 4% BSA was ~ 0.15 which indicates that besides albumin
20 an alternative plasma protein may be involved in the binding (assuming binding is similar to human
21 and bovine albumin). This may be α₁-acid glycoprotein, which binds mainly basic compounds.²⁰

22
23 The negligible uptake of both [¹¹C]**1** and [¹¹C]**7f** into the hCD80-positive xenografts may result
24 from the high plasma protein binding, hampering extravasation of the tracers. The small volume
25 of distribution, in particular of [¹¹C]**7f** (14 % of total body volume¹⁹) supports this hypothesis. The
26 pre-administration of cyclosporine reduced the biliary excretion significantly and in addition
27 increased the volume of distribution and tissue distribution, though without statistical
28 significance¹⁹. Both the reduction in spill-over from abdominal radioactivity and potential increase

1
2
3 in tissue distribution may have contributed to the observed increased radioactivity in peripheral
4 parts of the hCD80-rich xenografts in two out of four cyclosporine treated animals.
5
6

7
8 Biliary excretion as well as strong binding to plasma proteins may depend on the cationic
9 characteristics of the tracers^{21,22,23,24}. We currently investigate the effect of the charge and
10 ionization state on the binding affinity to hCD80, biliary excretion, plasma protein binding and
11 finally *in vivo* imaging.
12
13
14
15
16
17
18
19

20 21 CONCLUSION

22
23 A structure-affinity relationship study identified structural features which promote low nanomolar
24 affinity to hCD80. Despite strong *in vitro* binding of **7f** to hCD80, observed by SPR and
25 autoradiography, PET-tracer [¹¹C]**7f** hardly accumulated in hCD80-rich xenografts *in vivo*. High
26 plasma protein binding and high spill-over due to biliary excretion may have hampered observable
27 accumulation. Further structural modifications towards pharmacokinetic optimisation will be
28 based on these results. Besides imaging, our findings may be of interest for the development of
29 therapeutic CD80 inhibitors.
30
31
32
33
34
35
36
37
38
39
40
41
42
43
44
45
46
47
48
49
50
51
52
53
54
55
56
57
58
59
60

1
2
3 EXPERIMENTAL SECTION
4
5

6 **Materials & methods.** All chemicals, unless otherwise stated, were purchased from Sigma
7 Aldrich GmbH (Taufkirchen, Germany), ABCR GmbH (Karlsruhe, Germany), Merck (Darmstadt,
8 Germany), Fluorochem Ltd. (Hadfield, GB), Tokyo Chemical Industry Co. Ltd (Tokyo, Japan),
9 Apollo Scientific Ltd (Cheshire, GB) or Fisher Scientific International Inc. (Hampton, US) and
10 were used without further purification.
11
12

13 Solvents for thin layer chromatography (TLC), column chromatography and extractions were
14 commercial grade. Organic chemistry reactions were monitored by TLC using Sigma-Aldrich
15 silica gel 60 plates (UV light at 254 nm). Nuclear magnetic resonance (NMR) spectra (^1H and ^{13}C
16 NMR) were obtained on a Bruker Avance FT-NMR spectrometer (400 MHz). Chemical shifts are
17 given in delta (δ) units, in ppm relative to tetramethylsilane (TMS, 0 ppm). Multiplicities in the ^1H
18 NMR spectra are described as: s = singlet, d = doublet, t = triplet and m = multiplet. Coupling
19 constants (J) are reported in Hz. High resolution mass spectrometry (HR-MS) was performed by
20 the MS service of the Laboratory for Organic Chemistry at the ETH Zürich. The MALDI spectra
21 were recorded on a Bruker solariX (MALDI-FTICR-MS) or Bruker UltraFlex II (MALDI-TOF-
22 MS), while the ESI were recorded on a Bruker maXis (ESI-Qq-TOF-MS) or Bruker solariX (ESI-
23 FTICR-MS). High-performance liquid chromatography (HPLC) analysis was performed using a
24 reversed phase column (ACE column, C18, 3 μm) with a gradient system of acetonitrile and
25 50 mM sodium acetate. Semi-preparative HPLC purifications were carried out on a reversed phase
26 column (ACE column, Symmetry C8 5 μm ; 7.8 \times 50 mm) under following conditions: 4.1 g/L
27 sodium acetate in H_2O (solvent A), MeCN (solvent B); isocratic with 25% B; flow rate
28 4.5 mL/min. The UV signal was measured at a wavelength of 320 nm.
29
30
31
32
33
34
35
36
37
38
39
40
41
42
43
44
45
46
47
48
49
50
51
52
53
54
55
56
57
58
59
60

1
2
3 The purity of all biologically tested compounds was $\geq 95\%$, except of intermediate **6d** with a purity
4 of 92%. Purity was determined by HPLC using an analytical reverse phase column (Xbridge, C18,
5 5 μm ; 4.6 x 150mm) with H₂O/MeCN (both containing 0.1% TFA) as mobile phase. Method: 2 min
6 isocratic 5% MeCN followed by a gradient from 5% to 90% MeCN in 12 min. Peaks
7 corresponding to the desired product are described, including retention time (rt) and purity by
8 integration.
9

10
11
12 The recombinant human CTLA-4 fusion protein abatacept (Orencia[®], Bristol-Myers-Squibb) and
13 cyclosporine (Sandimmun[®], Novartis) were purchased from a local pharmacy.
14
15

16
17
18 All animal experiments were carried out in accordance with the Swiss Animal Welfare legislation
19 and approved by the Veterinary Office of the Canton Zurich (ZH17/2015 and ZH18/2018). Female
20 C.B.17 SCID mice (xenografts) and male C57BL/6 mice (tracer metabolism) were purchased from
21 Charles River Laboratories (Sulzfeld, Germany) and housed under standard conditions (12 h
22 light/12 h dark, free access to chow and water). [¹⁸F]FDG was generated in a routine production
23 by the University Hospital Zurich.
24
25
26
27
28
29
30
31
32
33
34
35

36 37 38 39 40 **Chemistry**

41
42
43 **4-(6-fluoro-1,3-dihydro-3-oxo-2H-pyrazolo[4,3-c]cinnolin-2-yl)-N-(1-methyl-4-piperidinyl)-**
44 **benzamide (1)**. Compound **1** was synthesised from **6b** following the same experimental procedure
45 like the synthesis of **2** and 1-methylpiperidine-4-amine. MS (ESI) calculated for C₂₂H₂₂FN₆O₂⁺:
46 421.2; *m/z* found was 421.2 [M+H]⁺; rt 9.36 min, 95%.
47
48
49
50
51
52
53
54
55
56
57
58
59
60

1
2
3 **4-[3,6-dihydro-6-methyl-3-oxo-4-[3-(trifluoromethyl)phenyl]dipyrazolo[3,4-*b*:3',4'-*d*]pyri-**
4 **din-2(1*H*)-yl]-*N*-[3-(1-hydroxyethyl)phenyl]-benzamide (2).** 100 mg (0.22 mmol) of **6c** were
5 dissolved in 1.1 mL DMF and stirred in a round-bottom flask. 93 mg (0.66 mmol) 1-(3-
6 aminophenyl)ethan-1-ol, 70 μ L (0.40 mmol) DIPEA and 85 mg (0.44 mmol) EDC hydrochloride
7 were added and the mixture was stirred for 7 h, before EtOAc and 0.25-M HCl was added, and
8 extraction was performed. The combined organic layers were washed with brine, dried over
9 sodium sulfate, filtered and concentrated. The crude was purified by flash chromatography (9:1
10 EtOAc:EtOH saturated with ammonium bicarbonate) and relevant fractions were collected and
11 concentrated, which resulted in a product weight of 78 mg (62% yield). HR-MS (ESI) calculated
12 for $C_{30}H_{24}F_3N_6NaO_3^+$: 595.1676; m/z found was 595.1675 $[M+Na]^+$; rt 13.58 min, 95%.

13
14
15
16
17
18
19
20
21
22
23
24
25
26
27
28
29
30 **2-chloro-5-[3,6-dihydro-6-methyl-3-oxo-4-[3-(trifluoromethyl)phenyl]dipyrazolo[3,4-*b*:3',**
31 **4'-*d*]pyridin-2(1*H*)-yl]-benzoic acid (3).** 64 mg (0.28 mmol) of 2-chloro-5-hydrazinylbenzoic
32 acid hydrochloride were dispersed in 480 μ L ethylene glycol, before 47.4 mg (0.47 mmol) of
33 sodium tert-butoxide were added and the mixture was stirred for 1.5 h at 75°C. It was cooled to rt
34 and 36 mg (0.09 mmol) of **5c** were added with 1 mL of tert-butanol. The mixture was heated at
35 reflux (100°C) for 30 h. After 23 h additional sodium tert-butoxide (85 mg, 0.84 mmol) and
36 another 10 mg (0.05 mmol) of 2-chloro-5-hydrazinylbenzoic acid hydrochloride were added. The
37 reaction was quenched with water and EtOAc. The pH was set to 3 with 0.5-M HCl. The combined
38 organic layers were washed with brine, dried over sodium sulfate, filtered and concentrated. The
39 crude was dissolved in 2-3 mL EtOAc and kept at 0°C for 72 h. Orange precipitation formed,
40 which was filtered and resulted in a product weight of 14.3 mg (31% yield). MS (ESI) calculated
41 for $C_{22}H_{14}ClF_3N_5O_3^+$: 488.1; m/z found 488.1 $[M+H]^+$; rt 13.64 min, 95%.

1
2
3
4
5
6 **Ethyl-3-methoxy-3-(3-(trifluoromethyl)phenyl)acrylate (4).** 5 mL (28 mmol) ethyl 3-
7
8 (trifluoro-methyl)benzoate were dissolved in 200 mL EtOAc. 1.13 mg (28 mmol) sodium hydride
9
10 was added under stirring and heated to 40°C for 5 min, before another 1.13 mg (28 mmol) sodium
11
12 hydride was added and the reaction mixture was heated under reflux (90°C) for 18 h. The reaction
13
14 was cooled to rt and DCM/water was added. Extraction was performed and the combined organic
15
16 layers were washed with brine, dried over sodium sulfate, filtered and concentrated. The crude was
17
18 further dried with benzene under reduced pressure. In a second step, the crude intermediate was
19
20 dissolved in 100 mL 4:1 MeCN:MeOH and 28 mL (56 mmol) 2-M (diazomethyl)trimethylsilane
21
22 in hexane was added. The reaction was stirred for 36 h at rt, before it was quenched with 8 mL
23
24 aqueous 1-M HCl and extraction was performed with EtOAc. The combined organic layers were
25
26 washed with brine, dried over sodium sulfate, filtered and concentrated, which resulted in 9.63 g
27
28 crude. Flash chromatography was performed with 95:5 hexane:EtOAc, resulting in a product
29
30 weight of 3.74 g (48% yield). ¹H NMR (400 MHz, Chloroform-*d*) δ 7.81 (s, 1H), 7.74 (d, *J* = 7.5
31
32 Hz, 1H), 7.68 (d, *J* = 7.5 Hz, 1H), 7.53 (t, *J* = 7.5 Hz, 1H), 5.63 (s, 1H), 4.22 (q, *J* = 7.1 Hz, 2H),
33
34 3.90 (s, 3H), 1.31 (t, *J* = 7.1 Hz, 4H). ¹⁹F NMR (376 MHz, Chloroform-*d*) δ -62.80. HR-MS (ESI)
35
36 calculated for C₁₃H₁₄F₃O₃⁺: 275.0890; *m/z* found was 275.0895 [M+H]⁺.
37
38
39
40
41
42
43
44
45

46 **Methyl 4-hydroxycinnoline-3-carboxylate (5a).** To a mixture of 6 mL (84 mmol)
47
48 thionylchloride and 10 mL chloroform, 4 g (19 mmol) of compound 2-(2-
49
50 phenylhydrazono)malonic acid was added. The reaction mixture was stirred at 80°C for two hours
51
52 under nitrogen atmosphere. The solvents were removed under vacuum and the brown residue was
53
54 re-dissolved in dichloroethane and dried again. The resulting acid chloride was dissolved in 10 mL
55
56
57
58
59
60

1
2
3 dichloroethane, then 1.2 mL TiCl_4 were added and the dark brown solution was stirred at 110°C
4
5 for 4 hours under nitrogen. The reaction mixture was cooled to 10°C , 20 mL methanol were added
6
7 slowly and the resulting red-brown solution was stirred at 60°C for 30 min. The solvents were
8
9 removed under reduced pressure and the residues were crystalized from 10 mL acetonitrile to yield
10
11 0.6 g of compound **5a** (15% yield). ^1H NMR (400 MHz, $\text{DMSO}-d_6$) δ 13.94 (s, 1H), 8.10 (d, $J =$
12
13 8.2 Hz, 1H), 7.84 (t, $J = 7.7$ Hz, 1H), 7.68 (d, $J = 8.2$ Hz, 1H), 7.52 (t, $J = 7.7$ Hz, 1H), 3.83 (s,
14
15 3H). MS (ESI) calculated for $\text{C}_{10}\text{H}_9\text{N}_2\text{O}_3^+$: 205.1; m/z found was 204.7 $[\text{M}+\text{H}]^+$.
16
17
18
19
20
21
22

23 **Methyl 4-hydroxy-8-fluorocinnoline-3-carboxylate (5b)**. Compound **5b** was synthesized in an
24
25 analogous way to the procedure for compound **5a**, but with 2-(2-(2-
26
27 fluorophenyl)hydrazono)malonic acid. ^1H NMR (400 MHz, $\text{DMSO}-d_6$) δ 14.19 (s, 1H), 7.90 (d, J
28
29 = 8.2 Hz, 1H), 7.77 (ddd, $J = 11.2, 8.0, 1.2$ Hz, 1H), 7.49 (td, $J = 8.1, 4.8$ Hz, 1H), 3.85 (s, 3H).
30
31 MS (ESI) calculated for $\text{C}_{10}\text{H}_8\text{FN}_2\text{O}_3^+$: 223.0; m/z found was 222.9 $[\text{M}+\text{H}]^+$.
32
33
34
35
36

37 **Ethyl 4-chloro-1-methyl-6-(3-(trifluoromethyl)phenyl)-1H-pyrazolo[3,4-*b*]pyridine-5-car-**
38
39 **boxylate (5c)**. This intermediate was synthesised from **4** following the same experimental
40
41 procedure like the synthesis of **5e** and ethyl 5-amino-1-methyl-1H-pyrazole-4-carboxylate,
42
43 resulting in a product weight of 830 mg (60% yield). ^1H NMR (400 MHz, Chloroform-*d*) δ 8.18
44
45 (s, 1H), 7.96 (s, 1H), 7.88 (d, $J = 7.8$ Hz, 1H), 7.73 (d, $J = 7.8$ Hz, 1H), 7.60 (t, $J = 7.8$ Hz, 1H),
46
47 4.22 (q, $J = 7.1$ Hz, 2H), 4.20 (s, 3H), 1.12 (t, $J = 7.1$ Hz, 3H). MS (ESI) calculated for
48
49 $\text{C}_{17}\text{H}_{14}\text{ClF}_3\text{N}_3\text{O}_2^+$: 384.1; m/z found was 384.2 $[\text{M}+\text{H}]^+$.
50
51
52
53
54
55
56
57
58
59
60

1
2
3 **Ethyl 4-chloro-2-(3-(trifluoromethyl)phenyl)quinoline-3-carboxylate (5d)**. This intermediate
4
5 was synthesised from **4** following the same experimental procedure like the synthesis of **5e** and
6
7 ethyl-2-aminobenzoate, resulting in a product weight of 418 mg (61% yield). ¹H NMR (400 MHz,
8
9 Chloroform-*d*) δ 8.32 (d, *J* = 8.4 Hz, 1H), 8.19 (d, *J* = 8.4 Hz, 1H), 8.03 (s, 1H), 7.95 (d, *J* = 7.8
10
11 Hz, 1H), 7.86 (t, *J* = 8.4 Hz, 1H), 7.77 – 7.69 (m, 2H), 7.62 (t, *J* = 7.8 Hz, 1H), 4.29 (q, *J* = 7.2
12
13 Hz, 2H), 1.18 (t, *J* = 7.2 Hz, 3H). ¹³C NMR (101 MHz, CDCl₃) δ 166.2, 154.7, 148.0, 141.2, 140.0,
14
15 132.0, 131.0, 130.1, 129.3, 128.8, 127.1, 126.9, 126.2, 125.6, 125.4, 124.7, 122.7, 62.6, 13.8. ¹⁹F
16
17 NMR (376 MHz, Chloroform-*d*) δ -62.68. HR-MS (ESI) was calculated for C₁₉H₁₃ClF₃NNaO₂⁺:
18
19 380.0660; *m/z* found was 380.0663 [M+H]⁺.
20
21
22
23
24
25
26

27 **Ethyl 4-chloro-8-fluoro-2-(3-(trifluoromethyl)phenyl)quinoline-3-carboxylate (5e)**. 740 mg
28
29 (4.4 mmol) of methyl 2-amino-3-fluorobenzoate were dissolved in 8 mL THF, before 193 mg
30
31 (4.8 mmol) sodium hydride was added and the mixture was stirred at room temperature. After
32
33 30 min, 1.20 g (4.4 mmol) of **4** with 1.7 mL THF was transferred to the mixture. The reaction was
34
35 run under reflux for 16 h, before it was cooled to room temperature and quenched with water. The
36
37 pH was set to 5 with aqueous HCl. Extraction was performed with EtOAc and the combined
38
39 organic fractions were dried, filtered and concentrated, which resulted in a crude weight of 1.86 g.
40
41 The crude was dissolved in 19 mL phosphorus oxychloride and stirred at reflux for 2 h. After
42
43 cooling to room temperature, it was concentrated under reduced pressure. The residues were
44
45 dissolved in EtOAc, cooled to 0°C and neutralised with aqueous 5% NaHCO₃. Extraction was
46
47 performed with EtOAc and the collected organic layers were dried over sodium sulfate and
48
49 concentrated, resulting in a crude weight of 1.81 g. Flash chromatography (9:1 Hexane:EtOAc)
50
51 was performed, giving a product weight of 955 mg (55% yield). ¹H NMR (400 MHz, Chloroform-
52
53
54
55
56
57
58
59
60

1
2
3 d) δ 8.12 (d, $J = 8.5$ Hz, 1H), 8.02 (s, 1H), 7.98 (d, $J = 7.7$ Hz, 1H), 7.75 (d, $J = 7.7$ Hz, 1H), 7.72
4
5 – 7.54 (m, 3H), 4.30 (q, $J = 7.1$ Hz, 1H), 3.84 (s, 2H), 1.19 (t, $J = 7.1$ Hz, 1H). ^{13}C NMR (101
6
7 MHz, CDCl_3) δ 165.9, 159.5, 156.9, 154.8, 139.7, 132.2, 129.5, 128.6, 128.5, 128.1, 126.4, 126.3,
8
9 125.6, 125.4, 122.7, 120.5, 116.2, 62.8, 13.8. ^{19}F NMR (376 MHz, Chloroform-*d*) δ -62.66, -
10
11 122.57. HR-MS (ESI) calculated for $\text{C}_{19}\text{H}_{13}\text{ClF}_4\text{NO}_2^+$: 398.0565; m/z found was 398.0565
12
13 $[\text{M}+\text{H}]^+$.
14
15
16
17
18
19

20 **4-(3-oxo-1,3-dihydro-2H-pyrazolo[4,3-*c*]cinnolin-2-yl)benzoic acid (6a)**. 0.5 g (2.4 mmol) of
21
22 compound **5a** were added in 2 mL (27 mmol) thionyl chloride and the reaction mixture was stirred
23
24 at 80°C for 1 h. The excess of thionyl chloride was removed under vacuum. The residue was
25
26 dissolved in toluene and the solvent was removed under vacuum to remove the traces of thionyl
27
28 chloride. Then 0.73 g (4.8 mmol) 4-hydrazinylbenzoic acid and 7 mL ethanol were added and the
29
30 reaction mixture was stirred at 70°C for 1 h. The resulting precipitates were collected and washed
31
32 with methanol:37% aqueous HCl mixture (9:1, 10 mL). The crude product was washed
33
34 additionally 3 times with water, methanol, and methylene chloride and dried to yield 0.57 g of
35
36 compound **6a** (78% yield). ^1H NMR (400 MHz, $\text{DMSO-}d_6$) δ 14.62 (s, 1H), 12.84 (s, 1H), 8.33 (d,
37
38 $J = 8.9$ Hz, 2H), 8.21 (d, $J = 7.8$ Hz, 1H), 8.06 (d, $J = 8.9$ Hz, 2H), 7.86 – 7.78 (m, 2H), 7.73 –
39
40 7.66 (m, 1H). MS (ESI) calculated for $\text{C}_{16}\text{H}_{11}\text{N}_4\text{O}_3^+$: 307.1; m/z found was 306.7 $[\text{M}+\text{H}]^+$; rt
41
42 10.78 min, >99%.
43
44
45
46
47
48
49
50

51 **4-(6-fluoro-3-oxo-1,3-dihydro-2H-pyrazolo[4,3-*c*]cinnolin-2-yl)benzoic acid (6b)**. The
52
53 structure was synthesised in an analogous way to the procedure of compound **6a** with compound
54
55 **5b** as starting material. ^1H NMR (400 MHz, $\text{DMSO-}d_6$) δ 14.71 (s, 1H), 12.87 (s, 1H), 8.26 (d, J
56
57
58
59
60

1
2
3 = 8.9 Hz, 2H), 8.02 (d, $J = 8.9$ Hz, 2H), 7.96 (d, $J = 7.8$ Hz, 1H), 7.73 – 7.58 (m, 2H). MS (ESI)
4
5 calculated for $C_{16}H_{11}FN_4O_3^+$: 325.1; m/z found was 324.7 $[M+H]^+$.
6
7
8
9

10
11 **4-(6-methyl-3-oxo-4-(3-(trifluoromethyl)phenyl)-3,6-dihydrodipyrzolo[3,4-*b*:3',4'-**

12 ***d*]pyridin-2(1*H*)-yl)benzoic acid (6c).** This intermediate was synthesised from **5c** following the
13 experimental procedure like the synthesis of **6e**, resulting in a product weight of 825 mg (85%
14 yield). 1H NMR (400 MHz, Acetone- d_6) δ 12.24 (s, 1H), 8.45 (s, 1H), 8.39 (d, $J = 7.8$ Hz, 1H),
15 8.22 (s, 1H), 8.12 (s, 4H), 7.87 (d, $J = 7.8$ Hz, 1H), 7.76 (t, $J = 7.8$ Hz, 1H), 4.16 (s, 3H). ^{19}F NMR
16 (376 MHz, Acetone- d_6) δ -62.88. HR-MS (ESI) calculated for $C_{22}H_{15}F_3N_5O_3^+$: 454.1122; m/z
17 found was 454.1128 $[M+H]^+$; rt 13.31 min, >99%.
18
19
20
21
22
23
24
25
26
27
28
29

30
31 **4-(3-oxo-4-(3-(trifluoromethyl)phenyl)-1,3-dihydro-2*H*-pyrazolo[4,3-*c*]quinolin-2-**

32 ***yl*)benzoic acid (6d).** This intermediate was synthesised from **5d** following the same experimental
33 procedure like the synthesis of **6e**, resulting in a product weight of 120 mg (68% yield). 1H NMR
34 (400 MHz, DMSO- d_6) δ 12.72 (s, 1H), 8.39 – 8.32 (m, 3H), 8.30 (d, $J = 7.6$ Hz, 1H), 8.25 (d, $J =$
35 7.8 Hz, 1H), 8.05 (d, $J = 7.8$ Hz, 1H), 8.01 (d, $J = 8.9$ Hz, 2H), 7.90 – 7.84 (m, 2H), 7.73 (t, $J =$
36 7.6 Hz, 1H), 7.60 (t, $J = 7.6$ Hz, 1H). ^{13}C NMR (101 MHz, DMSO- d_6) δ 167.5, 162.0, 151.3,
37 144.7, 143.9, 136.6, 134.7, 131.0, 130.9, 130.7, 129.7, 128.5, 127.4, 127.1, 126.1, 125.8, 123.1,
38 122.4, 120.3, 118.7 118.2, 102.6. ^{19}F NMR (376 MHz, DMSO- d_6) δ -60.96. MS (ESI) calculated
39 for $C_{24}H_{15}F_3N_3O_3^+$: 450.1; m/z found was 450.1 $[M+H]^+$; rt 13.35 min, 92%.
40
41
42
43
44
45
46
47
48
49
50
51
52
53
54
55
56
57
58
59
60

1
2
3 **4-(6-fluoro-3-oxo-4-(3-(trifluoromethyl)phenyl)-1,3-dihydro-2H-pyrazolo[4,3-c]quinolin-2-**
4 **yl)benzoic acid (6e).** 429 mg (2.82 mmol) of 4-hydrazinylbenzoic acid were dissolved in 4.7 mL
5
6 ethylene glycol, 279 mg (2.82 mmol) sodium tert-butoxide were added and stirred at 75°C for 1 h.
7
8 After cooling, 374 mg (0.94 mmol) of **5e** dissolved in 2.0 mL THF were added and the reaction
9
10 mixture was heated to 100°C. After 16 h, another 100 mg of sodium tert-butoxide was added and
11
12 stirred at 100°C for another 3 h. The reaction was quenched with H₂O and EtOAc. The crude
13
14 solution was acidified to pH 3 using 1-M HCl and extracted with EtOAc. The organic layers were
15
16 dried with sodium sulfate and concentrated, giving 54.4 mg crude. For purification, trituration was
17
18 performed as described in the synthesis for **7g**. In short, the crude was dissolved in acetone, few
19
20 1-M HCl was added and the solution was concentrated at 100 mbar at 40°C until precipitate
21
22 formed. The suspension was stored in the fridge for 1 h. Filtration, washing with 1-M HCl and
23
24 cold H₂O, and subsequent drying, resulted in a product weight of 288 mg (66% yield). ¹H NMR
25
26 (400 MHz, DMSO-*d*₆) δ 12.79 (s, 1H), 12.58 (s, 1H), 8.30 (d, *J* = 8.9 Hz, 2H), 8.24 (s, 1H), 8.17
27
28 (d, *J* = 7.8 Hz, 1H), 8.08 (d, *J* = 7.4 Hz, 1H), 8.04 – 7.95 (m, 3H), 7.81 (t, *J* = 7.8 Hz, 1H), 7.71 –
29
30 7.43 (m, 2H). ¹³C NMR (101 MHz, DMSO-*d*₆) δ 167.0, 161.3, 153.7, 151.9, 151.2, 143.5, 143.3,
31
32 134.6, 130.3, 128.8, 128.5, 128.2, 127.7, 127.2, 126.9 (d, *J* = 7.6 Hz), 125.7, 125.5, 122.8, 120.4,
33
34 117.7, 115.8 (d, *J* = 17.1 Hz), 103.1. ¹⁹F NMR (376 MHz, DMSO-*d*₆) δ -60.92, -124.46. HR-MS
35
36 (ESI) calculated for C₂₄H₁₄F₄N₃O₃⁺: 468.0966; *m/z* found was 468.0966 [M+H]⁺.
37
38
39
40
41
42
43
44
45
46
47

48 ***N*-(1-methylpiperidin-4-yl)-4-(3-oxo-1,3-dihydro-2H-pyrazolo[4,3-c]cinnolin-2-**
49 **yl)benzamide (7a).** 24.7 mg (0.08 mmol) of **6a** were dissolved in 850 μL 2:1 DCM/THF and
50
51 240 μL (3.3 mmol) thionylchloride was added. The mixture was stirred at reflux for 3 h. The
52
53 reaction was cooled down and solvents were evaporated under reduced pressure. Benzene was
54
55
56
57
58
59
60

1
2
3 added two times to remove solvent residues, resulting in a crude weight of 32.1 mg. This crude
4
5 was then resuspended in 200 μL DMF. 12.7 μL (0.10 mmol) 1-methylpiperidin-4-amine and
6
7 22.8 μL (0.16 mmol) triethylamine were mixed with 210 μL DMF in a separate flask and then
8
9 added to the reaction. After 20 hours, the reaction was stopped by adding aqueous HCl solution
10
11 and EtOAc, which led to the formation of precipitates. The precipitates were washed with aqueous
12
13 HCl solution and cold water. The precipitates were dissolved with ethanol/water and concentrated
14
15 to half the volume and stored in the fridge overnight. Orange precipitates formed and were filtered
16
17 and washed. The precipitates were treated with toluene and dried under high-vacuum to give a
18
19 final product weight of 6.4 mg (19% yield). ^1H NMR (400 MHz, $\text{DMSO-}d_6$) δ 8.35 (d, $J = 8.9$ Hz,
20
21 2H), 8.33 – 8.29 (m, 1H), 8.21 (d, $J = 8.0$, 1H), 7.97 (d, $J = 8.9$ Hz, 2H), 7.90 (d, $J = 8.0$ Hz, 1H),
22
23 7.78 (t, $J = 7.7$ Hz, 1H), 7.66 (t, $J = 7.7$ Hz, 1H), 3.96 – 3.83 (m, 1H), 3.14 – 3.03 (m, 2H), 2.57 –
24
25 2.51 (m, 2H), 2.45 (s, 3H), 1.94 – 1.86 (m, 2H), 1.79 – 1.66 (m, 2H). HR-MS (ESI) calculated for
26
27 $\text{C}_{22}\text{H}_{23}\text{N}_6\text{O}_2^+$: 403.1877; m/z found was 403.1875 $[\text{M}+\text{H}]^+$; rt 9.32 min, 97%.
28
29
30
31
32
33
34
35
36

37 **4-(6-fluoro-3-oxo-1,3-dihydro-2H-pyrazolo[4,3-*c*]cinnolin-2-yl)-N-(3-(1-**
38
39 **hydroxyethyl)phenyl)benzamide (7b)**. This structure was synthesised from 20 mg of **6b**
40
41 following the same experimental procedure like the synthesis of **7c**, resulting in a product weight
42
43 of 11 mg (40% yield). ^1H NMR (400 MHz, $\text{DMSO-}d_6$) δ 10.23 (s, 1H), 8.34 (d, $J = 8.9$ Hz, 2H),
44
45 8.13 (d, $J = 8.9$ Hz, 2H), 8.05 (d, $J = 7.6$ Hz, 1H), 7.77 (s, 1H), 7.77 (s, 1H), 7.76 – 7.64 (m, 3H),
46
47 7.29 (t, $J = 7.8$ Hz, 1H), 7.08 (d, $J = 7.8$ Hz, 1H), 5.19 (s, 1H), 4.72 (q, $J = 6.5$ Hz, 1H), 1.34 (d,
48
49 $J = 6.5$ Hz, 3H). ^{19}F NMR (376 MHz, $\text{DMSO-}d_6$) δ -125.47. HR-MS (MALDI/ESI) calculated for
50
51 $\text{C}_{24}\text{H}_{18}\text{FN}_5\text{NaO}_3^+$: 466.1286; m/z found was 466.1282 $[\text{M}+\text{Na}]^+$; rt 11.64 min, 98%.
52
53
54
55
56
57
58
59
60

***N*-(3-(1-hydroxyethyl)phenyl)-4-(3-oxo-1,3-dihydro-2*H*-pyrazolo[4,3-*c*]cinnolin-2-**

yl)benzamide (7c). 15 mg (0.05 mmol) of **6a** were dissolved in 600 μ L 2:1 DMF/THF and 21 mg (0.15 mmol) of 1-(3-aminophenyl)ethan-1-ol as well as 24 mg (0.12 mmol) 1-ethyl-3-(3-dimethylaminopropyl)carbo-diimid hydrochloride (EDC·HCl) were added. Afterwards, 16 μ L (0.09 mmol) DIPEA were added and the reaction was stirred for 16 h at room temperature, before the reaction was quenched by the addition of EtOAc and aqueous 0.25-M HCl. The organic layers were dried over sodium sulfate and concentrated, resulting in a crude weight of 35.1 mg. Flash chromatography (9:1 EtOAc/EtOH, saturated with NH_4HCO_3) was used for purification, which resulted in a product weight of 2.8 mg (13% yield). ^1H NMR (400 MHz, Acetone- d_6) δ 9.49 (s, 1H), 8.45 (d, $J = 8.9$ Hz, 2H), 8.38 (s, 1H), 8.32 (d, $J = 7.8$ Hz, 1H), 8.21 (d, $J = 7.8$ Hz, 1H), 8.12 (d, $J = 8.9$ Hz, 2H), 8.01 (d, $J = 7.8$ Hz, 1H), 7.92 – 7.81 (m, 2H), 7.79 (d, $J = 7.7$ Hz, 1H), 7.63 – 7.54 (m, 2H), 7.29 (t, $J = 7.7$ Hz, 1H), 7.13 (d, $J = 7.7$ Hz, 1H), 4.85 (q, $J = 6.4$ Hz, 1H), 4.17 (d, $J = 4.1$ Hz, 1H), 1.42 (d, $J = 6.4$ Hz, 3H). HR-MS (ESI) calculated for $\text{C}_{24}\text{H}_{19}\text{N}_5\text{NaO}_3^+$: 448.1380; m/z found was 448.1386 $[\text{M}+\text{Na}]^+$; rt 11.53 min, 95%.

4-(6-methyl-3-oxo-4-(3-(trifluoromethyl)phenyl)-3,6-dihydropyrazolo[3,4-*b*:3',4'-

d]pyridin-2(1*H*)-yl)-*N*-(1-methylpiperidin-4-yl)benzamide (7d). This structure was synthesised from 20 mg of **6c** following the same experimental procedure like the synthesis of **7c**, resulting in a product weight of 16 mg (66% yield). ^1H NMR (400 MHz, DMSO- d_6) δ 10.62 (s, 1H), 8.59 (d, $J = 7.5$ Hz, 1H), 8.35 – 8.24 (m, 3H), 8.12 – 7.98 (m, 4H), 7.89 (d, $J = 7.8$ Hz, 1H), 7.76 (t, $J = 7.8$ Hz, 1H), 4.11 (s, 3H), 4.08 – 3.97 (m, 1H), 3.46 – 3.42 (m, 3H), 3.15 – 3.01 (m, 2H), 2.79 – 2.68 (m, 2H), 2.07 – 1.90 (m, 4H). ^{19}F NMR (376 MHz, DMSO- d_6) δ -60.88. HR-MS (ESI) calculated for $\text{C}_{28}\text{H}_{27}\text{F}_3\text{N}_7\text{O}_2^+$: 550.2173; m/z found was 550.2167 $[\text{M}+\text{H}]^+$; rt 11.71 min, 97%.

1
2
3
4
5
6 ***N*-(1-methylpiperidin-4-yl)-4-(3-oxo-4-(3-(trifluoromethyl)phenyl)-1,3-dihydro-2H-**
7
8 **pyrazolo[4,3-*c*]quinolin-2-yl)benzamide (7e).** This intermediate was synthesised from **6d**
9 following the same experimental procedure like the synthesis of **7f**, resulting in a product weight
10 of 31 mg (66% yield). ¹H NMR (400 MHz, DMSO-*d*₆) δ 8.40 (s, 1H), 8.39 – 8.30 (m, 3H), 8.28
11 (d, *J* = 8.2 Hz, 2H), 7.98 (d, *J* = 7.8 Hz, 2H), 7.93 (d, *J* = 8.9 Hz, 2H), 7.87 – 7.77 (m, 2H), 7.66
12 (t, *J* = 7.6 Hz, 1H), 7.53 (t, *J* = 7.6 Hz, 1H), 3.94 – 3.81 (m, 1H), 3.15 – 2.96 (m, 2H), 2.49 – 2.33
13 (m, 4H), 1.93 – 1.84 (m, 2H), 1.76 – 1.63 (m, 2H). ¹³C NMR (101 MHz, DMSO-*d*₆) δ 165.3, 161.3,
14 152.1, 145.0, 143.7, 142.7, 134.2, 129.7, 129.1, 128.9, 128.7, 128.0, 127.1, 126.7, 125.9, 125.5,
15 124.2, 121.7, 119.6, 118.9, 117.5, 69.8, 53.7, 45.4, 44.5, 30.3, 29.0. ¹⁹F NMR (376 MHz, DMSO-
16 *d*₆) δ -60.87. HR-MS (ESI) calculated for C₃₀H₂₇F₃N₅O₂⁺: 546.2111; *m/z* found was 546.2113
17 [M+H]⁺; rt 11.53 min, >99%.

18
19
20
21
22
23
24
25
26
27
28
29
30
31
32
33
34
35 **4-(6-fluoro-3-oxo-4-(3-(trifluoromethyl)phenyl)-1,3-dihydro-2H-pyrazolo[4,3-*c*]quinolin-2-**
36 **yl)-*N*-(1-methylpiperidin-4-yl)benzamide (7f).** 19.4 mg (0.043 mmol) of **6e** were dissolved in
37 200 μL DMF and stirred in a round-bottom flask. 18.6 mg (0.047 mmol) HATU were added and
38 the mixture was cooled to 0°C. In a separate flask, 16.5 μL (0.13 mmol) 1-methylpiperidin-4-
39 amine and 20 μL (0.13 mmol) DIPEA were mixed with 90 μL DMF and the solution was added
40 dropwise into the reaction mixture at 0°C under vigorous stirring. The reaction was kept stirring
41 for 35 min, before it was quenched by adding 1-M HCl and transferred into an Erlenmeyer tube
42 with ice and brine. This mixture was kept one hour in the fridge and formed precipitates. The
43 suspension was filtered and the precipitates were washed with 1-M HCl. Afterwards, the
44 precipitates were dissolved with EtOH and run through a 0.45 μm filter. The clear yellow solution
45
46
47
48
49
50
51
52
53
54
55
56
57
58
59
60

1
2
3 was concentrated and dried under high-vacuum, which resulted in a product weight of 20.9 mg
4 (87% yield). For crystal structure check Supplementary Figure S10. ¹H NMR (400 MHz, DMSO-
5 *d*₆) δ 12.62 (s, 1H), 10.52 (s, 1H), 8.52 (d, *J* = 7.5 Hz, 1H), 8.26 (d, *J* = 8.9 Hz, 2H), 8.23 (s, 1H),
6
7 8.16 (d, *J* = 7.8 Hz, 1H), 8.13 (d, *J* = 7.6 Hz, 0H), 8.02 (d, *J* = 7.8 Hz, 1H), 7.97 (d, *J* = 8.9 Hz,
8
9 2H), 7.83 (t, *J* = 7.8 Hz, 1H), 7.70 – 7.55 (m, 2H), 4.09 – 3.97 (m, 1H), 3.50 (s, 3H), 3.44 – 3.36
10
11 (m, 2H), 3.16 – 2.99 (m, 2H), 2.07 – 1.86 (m, 4H). ¹⁹F NMR (376 MHz, DMSO-*d*₆) δ -60.91, -
12
13 124.48. HR-MS (MALDI/ESI) calculated for C₃₀H₂₆F₄N₅O₂⁺: 564.2017; *m/z* found was 564.2016
14
15 [M+H]⁺; rt 11.72 min, 97%.
16
17
18
19
20
21
22
23
24

25 **4-(6-fluoro-3-oxo-4-(3-(trifluoromethyl)phenyl)-1,3-dihydro-2H-pyrazolo[4,3-c]quinolin-2-**
26 **yl)-N-(3-(1-hydroxyethyl)phenyl)benzamide (7g).** 17.6 mg (0.04 mmol) of **6e** were dissolved in
27 190 μL DMF and stirred in a round-bottom flask. 16.2 mg (0.12 mmol) 1-(3-aminophenyl)ethan-
28 1-ol, 14.9 mg (0.08 mmol) EDC·HCl and 12 μL (0.07 mmol) DIPEA was added in this respective
29 order. The reaction mixture was stirred at room temperature for 18 h, before it was diluted with
30 EtOAc. The organic layers were partitioned with 0.4-M HCl, dried and concentrated. The crude
31 was dissolved in 5 mL Aceton and 0.5 mL 1-M HCl were subsequently added. The solution was
32 concentrated at 100 mbar at 40°C until red-orange precipitate formed and was stored in the fridge
33 for 1 h. Afterwards the suspension was filtered and the precipitates were washed with 1-M HCl
34 and cold H₂O. The precipitates were dissolved with 9:1 EtOAc:EtOH. The solution was
35 concentrated and dried under high-vacuum, which resulted in a product weight of 5.5 mg (25%
36 yield). ¹H NMR (400 MHz, Acetone-*d*₆) δ 9.49 (s, 1H), 8.45 (d, *J* = 9.0 Hz, 2H), 8.38 (s, 1H), 8.32
37 (d, *J* = 7.9 Hz, 1H), 8.21 (dt, *J* = 7.8, 1.3 Hz, 1H), 8.12 (d, *J* = 9.0 Hz, 2H), 8.01 (d, *J* = 8.0 Hz,
38 1H), 7.88 – 7.77 (m, 3H), 7.63 – 7.54 (m, 2H), 7.29 (t, *J* = 7.8 Hz, 1H), 7.13 (d, *J* = 7.8 Hz, 1H),
39
40
41
42
43
44
45
46
47
48
49
50
51
52
53
54
55
56
57
58
59
60

1
2
3 4.85 (q, $J = 6.1$ Hz, 1H), 4.17 (d, $J = 4.0$ Hz, 1H), 1.42 (d, $J = 6.4$ Hz, 3H). ^{19}F NMR (376 MHz,
4 Acetone- d_6) δ -63.05, -129.05. HR-MS (ESI) calculated for $\text{C}_{32}\text{H}_{22}\text{F}_4\text{N}_4\text{NaO}_3^+$: 609.1520; m/z
5
6 found was 609.1519 $[\text{M}+\text{Na}]^+$; rt 13.91 min, 98%.
7
8
9

10
11
12
13 **4-(6-fluoro-3-oxo-1,3-dihydro-2H-pyrazolo[4,3-c]cinnolin-2-yl)-N-(piperidin-4-**
14 **yl)benzamide (8a)**. Compound **8a** was synthesised from **6b** following the same experimental
15 procedure like the synthesis of **8b** and as described in the supplementary part of a previous
16 publication.⁶
17
18
19
20
21
22

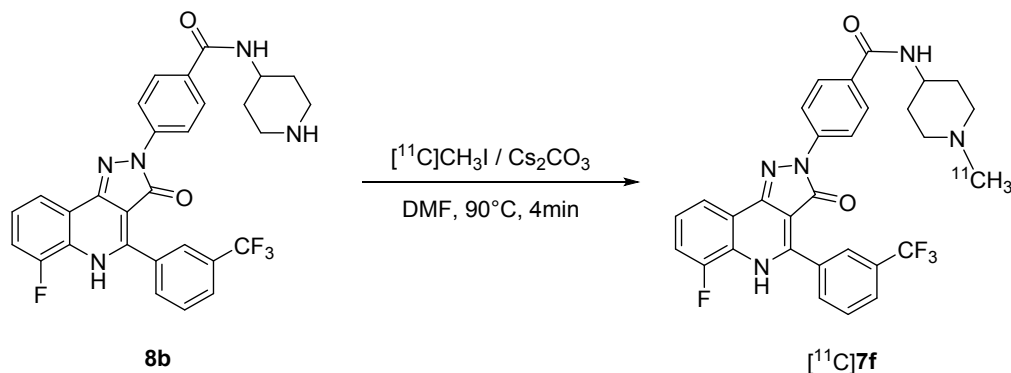
23
24
25
26 **4-(6-fluoro-3-oxo-4-(3-(trifluoromethyl)phenyl)-1,3-dihydro-2H-pyrazolo[4,3-c]quinolin-2-**
27 **yl)-N-(piperidin-4-yl)benzamide (8b)**. 16 mg (0.034 mmol) of **6e** were dissolved in 350 μL 2:1
28 DMF/THF. Afterwards, 8.0 mg (0.041 mmol) EDC·HCl, 41 μL (0.041 mmol) HOBt, 30 μL
29 (0.171 mmol) DIPEA and 17.1 mg (0.086 mmol) tert-butyl 4-aminopiperidine-1-carboxylate were
30 added in this respective order. The reaction was run for 22.5 h at room temperature. The mixture
31 was quenched with EtOAc and H_2O , and partitioned. The organic layers were dried over sodium
32 sulfate and concentrated, resulting in a crude weight of 51.1 mg. Flash chromatography (1:1
33 Hexane:EtOAc + 0.5% Acetic Acid) was performed for purification. After drying the product three
34 times with toluene, the weight of the intermediate was 20.1 mg. The intermediate was then
35 dissolved and stirred in DCM with 20% TFA for 1 h before concentrating under reduced pressure.
36 DCM and acidified water was added and an extraction was performed once. The water phase was
37 neutralised with aqueous 25% NH_3 solution and extraction with EtOAc was performed (5x). After
38 concentration under reduced pressure, this resulted in a product weight of 10.7 mg (70% yield).
39
40
41
42
43
44
45
46
47
48
49
50
51
52
53
54
55
56
57
58
59
60

¹H NMR (400 MHz, Methanol-*d*₄) δ 8.22 (s, 1H), 8.17 (d, *J* = 8.9 Hz, 2H), 8.13 (d, *J* = 7.8 Hz, 1H), 8.11 – 8.08 (m, 1H), 7.96 (d, *J* = 7.8 Hz, 1H), 7.85 (d, *J* = 8.9 Hz, 2H), 7.79 (t, *J* = 7.8 Hz, 1H), 7.54 – 7.47 (m, 1H), 7.46 – 7.38 (m, 1H), 4.21 – 4.11 (m, 1H), 3.52 – 3.44 (m, 2H), 3.20 – 3.10 (m, 2H), 2.25 – 2.16 (m, 2H), 1.94 – 1.82 (m, 2H). ¹³C NMR (101 MHz, Methanol-*d*₄) δ 169.2, 163.2, 155.2, 153.6, 152.7, 145.0, 143.6, 138.9, 135.1, 131.6, 131.2, 130.2, 129.9, 129.2, 128.2, 126.3, 121.9, 120.4, 119.2, 116.8, 116.6, 46.4, 44.4, 29.5. ¹⁹F NMR (376 MHz, Methanol-*d*₄) δ -63.92, -128.25. HR-MS (MADLI/ESI) calculated for C₂₉H₂₄F₄N₅O₂⁺: 550.1861; *m/z* found was 550.1861 [M+H]⁺.

Radiosynthesis of [¹¹C]1 and [¹¹C]7f. The radiotracers were synthesized as shown in Scheme 4 and as recently described for [¹¹C]1, with slight modifications.⁶ [¹¹C]CO₂ was produced by proton bombardment of nitrogen gas fortified with 0.5% oxygen in a Cyclone 18/9 cyclotron (18-MeV; IBA, Ottignies-Louvain-la-Neuve, Belgium) via the ¹⁴N(p,a)¹¹C nuclear reaction. In a first step, nickel-based catalytic reduction of [¹¹C]CO₂ yielded [¹¹C]methane which was subsequently iodinated to give [¹¹C]MeI. The [¹¹C]MeI was bubbled into a solution of 1.0 mg precursor (**8a** for [¹¹C]1 and **8b** for [¹¹C]7f, respectively) in 0.6 mL DMF and 5 mg cesium carbonate. The mixture was stirred at 90°C for 4 min. After dilution of the reaction with 1.6 mL 50 mM sodium acetate, the crude solution was purified by semi-preparative HPLC. The radiotracer was collected into 10 mL water and passed through a C18 cartridge. After washing with 5 mL water, the radiotracer was eluted with 0.5 mL ethanol into a sterile vial and diluted with 9.5 mL sterile 0.9% NaCl solution. For quality control, 100 μL of the final formulation was injected into the analytical HPLC system. Identity of the product was confirmed by comparison with the retention time of the

1
2
3 standard reference. The molar activity was calculated from the linear regression of a UV-intensity
4
5 based calibration curve of the cold reference.
6
7
8
9
10
11
12
13
14
15
16
17
18
19
20
21
22
23
24
25
26
27
28
29
30
31
32
33
34
35
36
37
38
39
40
41
42
43
44
45
46
47
48
49
50
51
52
53
54
55
56
57
58
59
60

Scheme 4. Radiosynthesis of [^{11}C]7f from precursor **8b**.



Radiosynthesis of [^{11}C]7f. Radiotracer [^{11}C]7f was prepared with precursor (**8b**) according to the above described radiosynthetic strategy of [^{11}C]1.⁶

Lipophilicity and lipid bilayer permeability. [^{11}C]7f (6 MBq in 20 μL) was mixed for 30 min in triplicates with 0.5 mL PBS-saturated 1-octanol and 0.5 mL PBS adjusted to pH 5.4, 7.4, 9.0 and 11.0, respectively. After centrifugation, 100 μL of each phase was measured in a gammacounter (Wizard, PerkinElmer) and $\log D$ was calculated as the logarithmic ratio between the 1-octanol and buffer phase. The data was analysed by non-linear regression with Equation 1:

$$D = \frac{P_i}{1 + 10^{(\text{pK}_a - \text{pH})}} + \frac{P_n}{1 + 10^{(\text{pH} - \text{pK}_a)}} \quad \text{Eq. 1}$$

where P_i and P_n are the lower and upper plateaux of the function, *i.e.*, P of the ionised and neutral species, respectively. The $\log P$ corresponds to the logarithmic P_n .

1
2
3 Lipid bilayer permeability (P_{FLipP}) was determined according to Hermann *et al.*¹⁸ with unilamellar
4
5 1-palmitoyl-2-oleoyl-*sn*-glycero-3-phosphocholine liposomes in 20 mM 3-morpholinopropane-
6
7 sulfonic acid/190 mM NaCl at pH 7.4.
8
9

10
11
12
13 **SPR affinity and displacement assays.** The SPR affinity assay was performed using a high
14
15 capacity amine chip with a dextran surface, which was activated using 1-ethyl-3-(3-
16
17 dimethylaminopropyl)carbodiimid and *N*-hydroxysuccinimid (EDC/NHS) and subsequently
18
19 coated with recombinant human CD80. The protein coated chip was kept under a steady flow of
20
21 running buffer (25 mM Tris, 150 mM NaCl, pH 7.2, containing 0.01% TWEEN® 20 and 5%
22
23 DMSO). The analytes were diluted with running buffer from a micromolar to a subnanomolar
24
25 concentration range. For the measurement, 100 μL of each dilution was injected with an injection
26
27 rate of 25 $\mu\text{L}/\text{min}$.
28
29
30

31
32
33 The SPR displacement assay was performed using an amine chip with a dextran surface, which
34
35 was activated using EDC/NHS and subsequently coated with rhCD80, rmCD80 or rhCD86. The
36
37 protein coated chip was kept under a steady flow of running buffer. The analytes were diluted with
38
39 2 nM rhCTLA-4 or 50 nM rhCD28 solutions in running buffer (25 mM Tris, 150 mM NaCl, pH
40
41 7.2, containing 0.01% TWEEN® 20 and 2.5% DMSO), from a micromolar to a subnanomolar
42
43 concentration range. For the measurement, 100 μL of each dilution was injected with an injection
44
45 rate of 25 $\mu\text{L}/\text{min}$.
46
47
48

49
50 All SPR experiments were carried out on a Sierra SPR-2 device (Sierra Sensors, Hamburg,
51
52 Germany). Data were analysed with the software Sierra Analyser (version 3.1.10.0). The Scrubber
53
54 software (version 2.0c, BioLogic Software, Canberra, Australia) revealed similar results (data not
55
56
57
58
59
60

1
2
3 shown). K_i values were estimated from the IC_{50} value, the K_d and the concentration of the displaced
4
5 ligand, according to the Cheng-Prusoff equation.²⁵
6
7
8
9

10
11 **Plasma protein binding.** For the evaluation of plasma protein binding, 0.5-1 MBq radiotracer was
12
13 added per 150 μ L plasma. The samples were incubated at room temperature for 10 min. To each
14
15 150 μ L radiotracer-plasma solution was added 300 μ L ice-cold PBS and all samples were briefly
16
17 vortexed. The samples were centrifuged at 14'000 x g in Amicon® Centrifugal Filters with a size
18
19 cutoff of 10 kDa for 15 min at 4°C. The filters were then inverted and briefly centrifuged at 200 x
20
21 g for 3 min to obtain the protein fraction. The radioactivity in Becquerel of the protein fraction
22
23 (A_{protein}), filtrate and filter unit were measured in a gammacounter (Wizard, PerkinElmer), A_{total}
24
25 was calculated as the sum of these radioactivities, and the free fraction f_u was calculated according
26
27 to equation 2:
28
29
30
31
32
33
34

$$f_u = 1 - \frac{A_{\text{protein}}}{A_{\text{total}}} \quad \text{Eq. 2}$$

35
36
37
38
39
40
41 **Animal xenograft model and PET/CT.** Raji cells (DSMZ, Braunschweig, Germany) were
42
43 cultured according to the supplier's recommendation. For inoculations, 2×10^6 Raji cells were
44
45 mixed with 100 μ L Matrigel (Corning Inc, US) and subcutaneously injected in the right shoulder
46
47 of SCID mice. PET/CT scans were performed 10 to 15 days after inoculation when the tumor
48
49 volume was between 1.25 and 1.76 cm^3 . For PET/CT imaging, mice were anesthetized by
50
51 inhalation of 2-5% isoflurane. Respiratory rate and body temperature were controlled as described
52
53 elsewhere.⁶ [^{11}C]7f (5-12 MBq, 13-19 nmol/kg) was injected intravenously into the tail vein and a
54
55
56
57
58
59
60

1
2
3 dynamic PET scan was run from 1 to 61 min post-injection with a subsequent CT scan, both on a
4 Super Argus PET/CT (Sedecal S.A., Madrid, Spain). Note that the same data sets were used in our
5
6 previous publication where details on data reconstruction are available.¹⁹ The reconstructed
7
8 PET/CT data were analysed using PMOD software (PMOD, Zurich, Switzerland; version 3.8).
9
10 Tissue radioactivity was expressed as standardized uptake values (SUV), which is the decay-
11
12 corrected image-derived radioactivity per cm³ tissue (multiplied with 1 g/cm³), divided by the
13
14 injected radioactivity dose per gram of body weight.
15
16
17
18
19
20
21
22

23 **In vivo metabolism of [¹¹C]7f.** [¹¹C]7f (55-74 MBq) was injected intravenously in three
24
25 15-16 weeks old male C57BL/6 mice. The mice were decapitated under isoflurane anaesthesia 15
26
27 min (2 animals) and 60 min (1 animal) after tracer injection and blood, bile and urine were
28
29 collected. Plasma was separated by centrifugation (1000 x g for 5 min at 4°C) and proteins were
30
31 denatured with an equal volume of MeCN on ice. After precipitation of the denatured proteins by
32
33 centrifugation, the filtrated supernatants were analysed by UHPLC. Bile and urine were mixed
34
35 with equal volumes of MeCN and filtrated for analysis by UHPLC. At 60 min post injection the
36
37 signal-to-noise ratio in plasma and urine were too low for evaluation.
38
39
40
41
42
43

44 **Single-crystal X-ray diffraction.** Structure was refined with SHELXL-2018/3 and
45
46 SHELXLE.^{26,27} Figure S10 was created with PLATON.²⁸ Data were collected at beamline PXI at
47
48 the Swiss Light Source, PSI. See CIF file for further details. CIF file deposited with CCDC
49
50 number 1937859.
51
52
53
54
55
56
57
58
59
60

1
2
3 **Statistical analysis.** Data were statistically evaluated with student's t test and non-linear curve
4 fitting with GraphPad Prism Software (Version 7.02, GraphPad Software Inc.) for IC50 or Excel
5 Solver (Microsoft Office 2016) for log *D*.
6
7
8
9
10
11
12
13
14
15
16
17
18
19
20
21
22
23
24
25
26
27
28
29
30
31
32
33
34
35
36
37
38
39
40
41
42
43
44
45
46
47
48
49
50
51
52
53
54
55
56
57
58
59
60

ANCILLARY INFORMATION

Supporting Information Availability

The Supporting Information is available free of charge on the ACS Publications website at <http://pubs.acs.org>.

- Molecular formula strings (CSV)
- Supporting material (PDF) containing:
 - [S1] SPR sensorgrams of the binding of **1** and **7f** to hCD80
 - [S2] SPR displacement of abatacept by compound **7f** on hCD86
 - [S3] SPR displacement of abatacept by compound **7f** on mCD80
 - [S4] pH-Dependent distribution of [¹¹C]**7f** between 1-octanol and PBS
 - [S5] Autoradiography with hCD80-positive & -negative xenograft slices with [¹¹C]**7f**
 - [S6] Quantification of autoradiographic experiment with [¹¹C]**7f**
 - [S7] Cell surface expression of hCD80, hCD86 and hCTLA-4 by flow cytometry
 - [S8] mRNA expression levels of hCD80/hCTLA-4/hCD28 in Raji and NCI xenografts
 - [S9] UHPLC chromatograms of *in vivo* samples from mice 15 min after [¹¹C]**7f** injection
 - [S10] Crystal data and structure refinement for compound **7f**

Corresponding Authors Information

Marco F. Taddio: marco.taddio@alumni.ethz.ch

Stefanie D. Krämer: stefanie.kraemer@pharma.ethz.ch

Acknowledgments

The authors thank Bruno Mancosu and Claudia Keller for their great technical support and their commitment with the radiotracer synthesis and subsequent animal studies and Peter Runge and

1
2
3 Cornelia Halin for their great support with the flow cytometry. This work was supported by the
4
5 Swiss National Science Foundation (SNSF) [153352 and 179238] and by the KFSP Molecular
6
7 Imaging Network Zurich (MINZ).
8
9

14 **Abbreviations used**

16
17 Bq, becquerel; CT, computed tomography; CTLA-4, cytotoxic T-lymphocyte-associated protein
18
19 4; DIPEA, *N,N*-diisopropylethylamine; EDC, 1-ethyl-3-(3-dimethylaminopropyl)carbodiimide;
20
21 EtOAc, ethyl acetate; EtOH, ethanol; FDG, fludeoxyglucose; HATU, 1-
22
23 [bis(dimethylamino)methylene]-1H-1,2,3-triazolo[4,5-b]pyridinium 3-oxid hexafluorophosphate;
24
25 HR-MS, high resolution mass spectrometry; HOBt, hydroxybenzotriazole; K_d , dissociation
26
27 constant; kDa, kilodalton; MeCN, acetonitrile; MeOH, methanol; NHS, *N*-hydroxysuccinimide;
28
29 RT-qPCR, real-time polymerase chain reaction; SPR, surface plasmon resonance; SUV,
30
31 standardized uptake value.
32
33
34
35
36
37
38
39
40
41
42
43
44
45
46
47
48
49
50
51
52
53
54
55
56
57
58
59
60

REFERENCES

- (1) Tivol, E. A.; Borriello, F.; Schweitzer, A. N.; Lynch, W. P.; Bluestone, J. A.; Sharpe, A. H. Loss of CTLA-4 Leads to Massive Lymphoproliferation and Fatal Multiorgan Tissue Destruction, Revealing a Critical Negative Regulatory Role of CTLA-4. *Immunity* **1995**, *3* (5), 541–547. [https://doi.org/10.1016/1074-7613\(95\)90125-6](https://doi.org/10.1016/1074-7613(95)90125-6).
- (2) Chen, L.; Flies, D. B. Molecular Mechanisms of T Cell Co-Stimulation and Co-Inhibition. *Nature Reviews Immunology*. 2013, pp 227–242. <https://doi.org/10.1038/nri3405>.
- (3) Schietinger, A.; Greenberg, P. D. Tolerance and Exhaustion: Defining Mechanisms of T Cell Dysfunction. *Trends in Immunology*. 2014, pp 51–60. <https://doi.org/10.1016/j.it.2013.10.001>.
- (4) Seliger, B.; Marincola, F. M.; Ferrone, S.; Abken, H. The Complex Role of B7 Molecules in Tumor Immunology. *Trends in Molecular Medicine*. 2008, pp 550–559. <https://doi.org/10.1016/j.molmed.2008.09.010>.
- (5) Dietel, B.; Altendorf, R.; Cicha, I.; Garlich, C. Migration of Regulatory T Cells into Human Atherosclerotic Lesions Is Associated with Plaque Stability and Correlates Inversely with Infiltrated Mature Dendritic Cells. *Eur. Heart J.* **2013**, *34*, 441.
- (6) Müller, A.; Mu, L.; Meletta, R.; Beck, K.; Rancic, Z.; Drandarov, K.; Kaufmann, P. A.; Ametamey, S. M.; Schibli, R.; Borel, N.; Krämer, S. D. Towards Non-Invasive Imaging of Vulnerable Atherosclerotic Plaques by Targeting Co-Stimulatory Molecules. *Int. J. Cardiol.* **2014**, *174* (3), 503–515. <https://doi.org/10.1016/j.ijcard.2014.04.071>.
- (7) Adams, A. B.; Ford, M. L.; Larsen, C. P. Costimulation Blockade in Autoimmunity

1
2
3 Costimulation Blockade in Autoimmunity and Transplantation: The CD28 Pathway. *J Immunol*
4 **2016**, *197* (6), 2045–2050. <https://doi.org/10.4049/jimmunol.1601135>.

7
8 (8) Biancone, L.; Segoloni, G.; Turello, E.; Donati, D.; Bussolati, B.; Piccoli, G.; Camussi, G.
9
10 Expression of Inducible Lymphocyte Costimulatory Molecules in Human Renal Allograft.
11
12 *Nephrol. Dial. Transplant* **1998**, *13* (3), 716–722.

15
16 (9) Kremer, J. M.; Westhovens, R.; Leon, M.; Di Giorgio, E.; Alten, R.; Steinfeld, S.; Russell,
17
18 A.; Dougados, M.; Emery, P.; Nuamah, I. F.; Williams, G. R.; Becker, J. C.; Hagerty, D. T.;
19
20 Moreland, L. W. Treatment of Rheumatoid Arthritis by Selective Inhibition of T-Cell Activation
21
22 with Fusion Protein CTLA4Ig. *N. Engl. J. Med.* **2003**, *349* (20), 1907–1915.
23
24 <https://doi.org/10.1056/nejmoa035075>.

27
28 (10) Cutolo, M.; Nadler, S. G. Advances in CTLA-4-Ig-Mediated Modulation of Inflammatory
29
30 Cell and Immune Response Activation in Rheumatoid Arthritis. *Autoimmunity Reviews*. 2013, pp
31
32 758–767. <https://doi.org/10.1016/j.autrev.2013.01.001>.

35
36 (11) Larsen, C. P.; Pearson, T. C.; Adams, A. B.; Tso, P.; Shirasugi, N.; Strobert, E.; Anderson,
37
38 D.; Cowan, S.; Price, K.; Naemura, J.; Emswiler, J.; Greene, J.; Turk, L. A.; Bajorath, J.;
39
40 Townsend, R.; Hagerty, D.; Linsley, P. S.; Peach, R. J. Rational Development of LEA29Y
41
42 (Belatacept), a High-Affinity Variant of CTLA4-Ig with Potent Immunosuppressive Properties.
43
44 *Am. J. Transplant.* **2005**, *5* (3), 443–453. <https://doi.org/10.1111/j.1600-6143.2005.00749.x>.

47
48 (12) Rostaing, L.; Vincenti, F.; Grinyó, J.; Rice, K. M.; Bresnahan, B.; Steinberg, S.; Gang, S.;
49
50 Gaithe, L. E.; Moal, M. C.; Mondragón-Ramirez, G. A.; Kothari, J.; Pupim, L.; Larsen, C. P. Long-
51
52 Term Belatacept Exposure Maintains Efficacy and Safety at 5 Years: Results from the Long-Term
53
54 Extension of the BENEFIT Study. *Am. J. Transplant.* **2013**, *13* (11), 2875–2883.

1
2
3 <https://doi.org/10.1111/ajt.12460>.

4
5
6 (13) Erbe, D. V.; Wang, S.; Xing, Y.; Tobin, J. F. Small Molecule Ligands Define a Binding
7 Site on the Immune Regulatory Protein B7.1. *J. Biol. Chem.* **2002**, *277* (9), 7363–7368.
8
9 <https://doi.org/10.1074/jbc.M110162200>.

10
11
12
13
14 (14) Green, N. J.; Xiang, J.; Chen, J.; Chen, L.; Davies, A. M.; Erbe, D.; Tam, S.; Tobin, J. F.
15 Structure-Activity Studies of a Series of dipyrazolo[3,4-b:3',4'-d]pyridin-3-Ones Binding to the
16 Immune Regulatory Protein B7.1. *Bioorganic Med. Chem.* **2003**, *11* (13), 2991–3013.
17
18
19 [https://doi.org/10.1016/S0968-0896\(03\)00183-4](https://doi.org/10.1016/S0968-0896(03)00183-4).

20
21
22
23
24 (15) Huxley, P.; Sutton, D. H.; Debnam, P.; Matthews, I. R.; Brewer, J. E.; Rose, J.; Trickett,
25 M.; Williams, D. D.; Andersen, T. B.; Classon, B. J. High-Affinity Small Molecule Inhibitors of
26 T Cell Costimulation: Compounds for Immunotherapy. *Chem. Biol.* **2004**, *11* (12), 1651–1658.
27
28
29 <https://doi.org/10.1016/j.chembiol.2004.09.011>.

30
31
32
33
34 (16) Uvebrant, K.; Da, D.; Thrige, G.; Rosén, A.; Åkesson, M.; Berg, H.; Walse, B.; Björk, P.
35 Discovery of Selective Small-Molecule CD80 Inhibitors. *J. Biomol. Screen.* **2007**, *12* (4), 464–
36
37
38
39 472. <https://doi.org/10.1177/1087057107300464>.

40
41
42 (17) Li, K.; Cheng, X.; Tilevik, A.; Davis, S. J.; Zhu, C. In Situ and in Silico Kinetic Analyses
43 of Programmed Cell Death-1 (PD-1) Receptor, Programmed Cell Death Ligands, and B7-1 Protein
44 Interaction Network. *J. Biol. Chem.* **2017**, *292* (16), 6799–6809.
45
46
47
48 <https://doi.org/10.1074/jbc.M116.763888>.

49
50
51 (18) Hermann, K. F.; Neuhaus, C. S.; Micallef, V.; Wagner, B.; Hatibovic, M.; Aschmann, H.
52 E.; Paech, F.; Alvarez-Sanchez, R.; Krämer, S. D.; Belli, S. Kinetics of Lipid Bilayer Permeation
53
54
55
56
57
58
59
60

1
2
3 of a Series of Ionisable Drugs and Their Correlation with Human Transporter-Independent
4 Intestinal Permeability. *Eur. J. Pharm. Sci.* **2017**, *104*, 150–161.
5
6 <https://doi.org/10.1016/j.ejps.2017.03.040>.
7
8

9
10
11 (19) Taddio, M. F.; Mu, L.; Keller, C.; Schibli, R.; Krämer, S. D. Physiologically Based
12 Pharmacokinetic Modelling with Dynamic PET Data to Study the in Vivo Effects of Transporter
13 Inhibition on Hepatobiliary Clearance in Mice. *Contrast Media Mol. Imaging* **2018**, Article ID
14 5849047. <https://doi.org/10.1155/2018/5849047>.
15
16
17
18

19
20
21 (20) Paxton, J. W. Alpha1-Acid Glycoprotein and Binding of Basic Drugs. *Methods and*
22 *Findings in Experimental and Clinical Pharmacology*. 1983, pp 635–648.
23
24

25
26 (21) Neef, C.; Meijer, D. K. F. Structure-Pharmacokinetics Relationship of Quaternary
27 Ammonium Compounds. *Naunyn. Schmiedebergs. Arch. Pharmacol.* **2004**, *328* (2), 111–118.
28
29 <https://doi.org/10.1007/bf00512059>.
30
31
32

33
34 (22) Jonker, J. W.; Wagenaar, E.; Mol, C. A. A. M.; Buitelaar, M.; Koepsell, H.; Smit, J. W.;
35 Schinkel, A. H. Reduced Hepatic Uptake and Intestinal Excretion of Organic Cations in Mice with
36 a Targeted Disruption of the Organic Cation Transporter 1 (Oct1 [Slc22a1]) Gene. *Mol. Cell. Biol.*
37 **2001**, *21* (16), 5471–5477. <https://doi.org/10.1128/MCB.21.16.5471>.
38
39
40
41
42

43
44 (23) Urien, S.; Tillement, J.-P. pH-Dependency of Basic Ligand Binding to alpha1-Acid
45 Glycoprotein (Orosomuroid). *Biochem. J.* **1991**, *280*, 277–280.
46
47 <https://doi.org/10.1042/bj2800277>.
48
49

50
51 (24) Huang, Z.; Ung, T. Effect of Alpha-1-Acid Glycoprotein Binding on Pharmacokinetics and
52 Pharmacodynamics. *Curr. Drug Metab.* **2013**, *14* (2), 226–238.
53
54
55

- 1
2
3 (25) Yung-Chi, C.; Prusoff, W. H. Relationship between the Inhibition Constant (KI) and the
4 Concentration of Inhibitor Which Causes 50 per Cent Inhibition (I50) of an Enzymatic Reaction.
5
6 *Biochem. Pharmacol.* **1973**, *22* (23), 3099–3108. [https://doi.org/10.1016/0006-2952\(73\)90196-2](https://doi.org/10.1016/0006-2952(73)90196-2).
7
8
9
10 (26) Sheldrick, G. M. Crystal Structure Refinement with SHELXL. *Acta Crystallogr. Sect. C*
11 *Struct. Chem.* **2015**, *71*, 3–8. <https://doi.org/10.1107/S2053229614024218>.
12
13
14
15 (27) Hübschle, C. B.; Sheldrick, G. M.; Dittrich, B. ShelXle: A Qt Graphical User Interface for
16 SHELXL. *J. Appl. Crystallogr.* **2011**, *44* (6), 1281–1284.
17
18
19 <https://doi.org/10.1107/S0021889811043202>.
20
21
22
23 (28) Spek, A. L. PLATON SQUEEZE: A Tool for the Calculation of the Disordered Solvent
24 Contribution to the Calculated Structure Factors. *Acta Crystallogr. Sect. C Struct. Chem.* **2015**, *71*,
25
26
27
28
29
30
31
32
33
34
35
36
37
38
39
40
41
42
43
44
45
46
47
48
49
50
51
52
53
54
55
56
57
58
59
60

